Proteomic analysis reveals that wildtype and alanine-expanded nuclear poly(A)-binding protein exhibit differential interactions in skeletal muscle

Received for publication, December 23, 2018, and in revised form, February 19, 2019 Published, Papers in Press, March 5, 2019, DOI 10.1074/jbc.RA118.007287

Ayan Banerjee[‡1], **Brittany L. Phillips**[‡§], **Quidong Deng**[¶], **Nicholas T. Seyfried**[¶], **Grace K. Pavlath**[‖], **Katherine E. Vest**[**2], **and Anita H. Corbett**[‡3]

From the [‡]*Department of Biology and the* [§]*Graduate Program in Genetics and Molecular Biology, Emory University, Atlanta, Georgia 30322 , the* [¶]*Department of Biochemistry, Center for Neurodegenerative Diseases and the* [‖]*Department of Pharmacology, Emory University School of Medicine, Atlanta, Georgia 30322, and the* [**]*Department of Molecular Genetics, Biochemistry & Microbiology, University of Cincinnati College of Medicine, Cincinnati, Ohio 45267*

Edited by Ronald C. Wek

Oculopharyngeal muscular dystrophy (OPMD) is a late-onset, primarily autosomal dominant disease caused by a short GCN expansion in the *PABPN1* (*polyadenylate-binding protein nuclear 1*) gene that results in an alanine expansion at the N terminus of the PABPN1 protein. Expression of alanine-expanded PABPN1 is linked to the formation of nuclear aggregates in tissues from individuals with OPMD. However, as with other nuclear aggregate-associated diseases, controversy exists over whether these aggregates are the direct cause of pathology. An emerging hypothesis is that a loss of PABPN1 function and/or aberrant protein interactions contribute to pathology in OPMD. Here, we present the first global proteomic analysis of the protein interactions of WT and alanine-expanded PABPN1 in skeletal muscle tissue. These data provide both insight into the function of PABPN1 in muscle and evidence that the alanine expansion alters the protein–protein interactions of PABPN1. We extended this analysis to demonstrate altered complex formation with and loss of function of TDP-43 (TAR DNA-binding protein 43), which we show interacts with alanine-expanded but not WT PABPN1. The results from our study support a model where altered protein interactions with alanine-expanded PABPN1 that lead to loss or gain of function could contribute to pathology in OPMD.

Polyalanine expansion diseases are caused by an abnormal number of *GCN* trinucleotide repeats that give rise to protein variants with expanded alanine tracts (1, 2). Oculopharyngeal muscular dystrophy (OPMD),[4] a late-onset muscle disease, is one such polyalanine expansion disorder that results from expansion of *GCN* trinucleotide repeats in the gene encoding the nuclear poly(A)-binding protein, PABPN1 (3). The N-terminal domain of PABPN1 contains a 10-alanine tract of unknown function that directly follows the initial methionine. In individuals with OPMD, this 10-alanine tract is expanded to 11–18 alanine residues with the most common disease variant containing a 13-alanine tract (3, 4). OPMD is commonly inherited in an autosomal dominant manner, so only a single modestly expanded copy of *PABPN1* is sufficient to confer pathology in a subset of skeletal muscles (3). How such a modest change in a single copy of the ubiquitously expressed *PABPN1* gene causes muscle-specific pathology is poorly understood.

Like other polyalanine expansion diseases, OPMD is characterized by the formation of insoluble protein aggregates (5). In OPMD, these aggregates are found in the nucleus and contain PABPN1, polyadenylated RNA, and other RNA-binding proteins (6, 7). Whether the formation of these PABPN1 aggregates causes toxicity and cell death or is a protective mechanism is unclear (8). However, the presence of nuclear PABPN1 aggregates in unaffected muscles and neurons (9–12) argues against a model based solely on aggregate-mediated toxicity. In fact, recent studies suggest that the pathogenic mechanism of OPMD is related to sequestration of PABPN1, other proteins, and RNAs in nuclear aggregates, thus decreasing the functional pools of these important molecules (7, 13, 14). Given that PABPN1 protein levels in muscle are already low (15), sequestration into aggregates or interaction with alanine-expanded PABPN1 may decrease available PABPN1 below some threshold required for normal muscle function (15, 16). If alanine expansion also impairs normal PABPN1 function, this could compound any defects associated with decreased PABPN1

This work was supported by National Institutes of Health Grants 5RO1AR061987 (to A. H. C. and G. K. P.) and 5F32AR068207 (to K.E.V.) and Muscular Dystrophy Association Grants 255856 (to A. B.) and 422006 (to A. H. C.). The authors declare that they have no conflicts of interest with the contents of this article. The content is solely the responsibility of the authors and does not necessarily represent the official views of the National Institutes of Health.

This article contains Table S1.

[1] Present address: Mitobridge (An Astellas Company), 1030 Massachusetts Ave., Suite 200, Cambridge, MA 02138.

[2] To whom correspondence may be addressed: Dept. of Molecular Genetics, Biochemistry & Microbiology, University of Cincinnati College of Medicine, Cincinnati, OH 45267. Tel.: 513-558-0023; E-mail: katherine.vest@uc.edu.

[3] To whom correspondence may be addressed: Dept. of Biology, Emory University, Atlanta, GA 30322. Tel.: 404-421-9061; E-mail: acorbe2@emory.edu.

[4] The abbreviations used are: OPMD, oculopharyngeal muscular dystrophy; DAPI, 4′,6′-diamino-2-phenylindole; GO, Gene Ontology; HMW, high-molecular-weight; PGRN, progranulin; 2-NBDG, 2-(*N*-(7-nitrobenz-2-oxa-1,3-diazol-4-yl)amino)-2-deoxyglucose; N-TAP, N-terminally TAP-tagged; C-TAP, C-terminally TAP-tagged; ALS, amyotrophic lateral sclerosis; DMEM, Dulbecco's modified Eagle's medium; FBS, fetal bovine serum; IP, immunoprecipitation; TAP, tandem affinity purification; MACS, magnetic-activated cell sorting.

availability and exacerbate pathology. However, few studies have probed how alanine expansion affects the function of the PABPN1 protein in muscle tissue *in vivo*.

As is true for many RNA-binding proteins (17), PABPN1 performs multiple critical functions in post-transcriptional regulation of gene expression (18). The canonical function of PABPN1 is enhancing the processivity of poly(A) polymerase during poly(A) tail addition to nascent RNAs (19). However, PABPN1 also plays important roles in polyadenylation and cleavage sequence selection (20, 21), nuclear export (22, 23), and the pioneer round of translation in the cytoplasm (24). Considering that alanine domains have been implicated in protein–protein interactions (25, 26), alanine expansion could affect interactions between PABPN1 and other proteins important for mediating these processes. For example, alanine-expanded PABPN1 could make abnormal protein contacts that lead to either a loss or gain of function. Alternatively, alanine-expanded PABPN1 could fail to interact with a subset of proteins critical for the proper function of PABPN1. A previous report demonstrated increased binding of alanine-expanded human PABPN1 to heat-shock proteins and arginine methyltransferases in lysates of C2C12 myoblasts and myotubes, supporting a model where alanine-expansion alters protein interactions with PABPN1 (27).

There is limited knowledge about PABPN1 functional interactions in skeletal muscle (28, 29). Characterizing and comparing the protein–protein interactions of WT and alanine-expanded PABPN1 in skeletal muscle tissue could provide valuable insight into the muscle-specific functions of PABPN1 while also identifying pathways most susceptible to dysfunction in OPMD. Here, we present the first global comparison of the protein interactions of WT and alanine-expanded PABPN1 expressed in skeletal muscle tissue. We detected an increased number of proteins associated with the alanine-expanded PABPN1 compared with WT PABPN1. Among the proteins that interact preferentially with alanine-expanded PABPN1 is the ALS-associated protein TDP-43, which forms aggregates in OPMD (30), associates with PABPN1 in neurons (31) and has recently been linked to key functions in regenerating muscle (32). The present study reveals that soluble TDP-43 is associated with higher-molecular-weight complexes and that TDP-43 is prone to oxidative stress-mediated aggregation in primary myoblasts that express alanine-expanded PABPN1. We also demonstrate alternative splicing of known TDP-43 targets, which suggests a loss of TDP-43 function. In addition to TDP-43, we identify other putative PABPN1 interactors that could be predisposed to dysfunction via a similar mechanism. This study provides both a comprehensive list of PABPN1-interacting proteins in skeletal muscle and insight into how these interactions are altered for alanine-expanded PABPN1. Our analysis also provides proof of principle that aberrant interactions with alanine-expanded PABPN1 can lead to changes in downstream cellular functions.

Results

Electroporation can be used to express epitope-tagged PABPN1 in skeletal muscle

Levels of PABPN1 protein are very low in skeletal muscle (15), making biochemical studies of PABPN1 protein interactions in this disease-relevant tissue challenging (29). Although several mouse models exist that express PABPN1, they either express native levels of alanine-expanded PABPN1 (33) or do not equally overexpress WT and alanine-expanded PABPN1 (34, 35). Thus, we used electroporation into skeletal muscle to allow direct comparison of the proteins that interact with WT PABPN1 and alanine-expanded PABPN1 in skeletal muscle.

To obtain skeletal muscle samples expressing equal levels of WT (Ala-10) PABPN1 and alanine-expanded (Ala-17) PABPN1, pcDNA3 plasmids encoding FLAG-tagged WT (Ala-10) or alanine-expanded (Ala-17) PABPN1 were electroporated into WT C56 Bl/6 mouse skeletal muscle (Fig. 1*A*). As a control, empty pcDNA3 plasmid was employed. Equal expression of WT and alanine-expanded PABPN1 was confirmed by immunoblotting with an anti-FLAG antibody (Fig. 1*B*). Expression of alanine-expanded PABPN1 was further confirmed by immunoblotting with an antibody specific to alanine-expanded PABPN1 (36).

To confirm the proper localization of exogenously expressed PABPN1, plasmids expressing GFP-tagged WT or alanine-expanded PABPN1 were electroporated into gastrocnemius muscle. As shown in Fig. 1*C*, GFP signal co-localizes with the DAPI signal at the position of muscle cell nuclei in muscle sections confirming the expected nuclear localization of both Ala-10 and Ala-17 PABPN1 in electroporated muscle.

Differential protein interactions with WT and alanine-expanded PABPN1

To identify PABPN1-interacting proteins, soluble FLAG-tagged Ala-10 and Ala-17 PABPN1 were immunoprecipitated from the electroporated skeletal muscle tissue, and bound samples were analyzed by MS as illustrated in the schematic shown in Fig. 1*A*. We first confirmed comparable immunoprecipitation of Ala-10 and Ala-17 PABPN1 (Table S1 and see Fig. 4*B*) and then analyzed the co-immunoprecipitating proteins. Mass spectrometry revealed a total of 381 proteins that were enriched in the FLAG-immunoprecipitations from muscle lysates expressing FLAG-tagged Ala-10 or Ala-17 PABPN1 but not from muscle lysates electroporated with the control pcDNA3 plasmid. PABPN1-interacting proteins were defined as those with a 2-fold or greater increase in FLAG immunoprecipitations in samples expressing FLAG–Ala-10 or FLAG–Ala-17 PABPN1 relative to control muscles (Table S1). A threshold of 2-fold or greater difference in the number of peptides co-immunoprecipitating with Ala-10 *versus* Ala-17 PABPN1 was used to define proteins as preferentially interacting with Ala-10 or Ala-17 PABPN1. Notably, the C-terminal domain of PABPN1 is required for RNA binding (37), and there is evidence that Ala-10 and Ala-17 PABPN1 interact to the same extent with RNA (38). Thus, these differential interactions are not likely to reflect RNA-dependent interactions.

Using the defined criteria, we identified 165 proteins that immunoprecipitated in approximately the same amount with both Ala-10 and Ala-17 PABPN1 (Ala-10 $\approx$ Ala-17), 49 proteins that immunoprecipitated more with Ala-10 PABPN1 than Ala-17 PABPN1 (Ala-10 $>$ Ala-17), and 167 proteins that immunoprecipitated more with Ala-17 than Ala-10 PABPN1 (Ala-17 $>$ Ala-10) (Fig. 2*A* and Table S1). Of these, 30 proteins

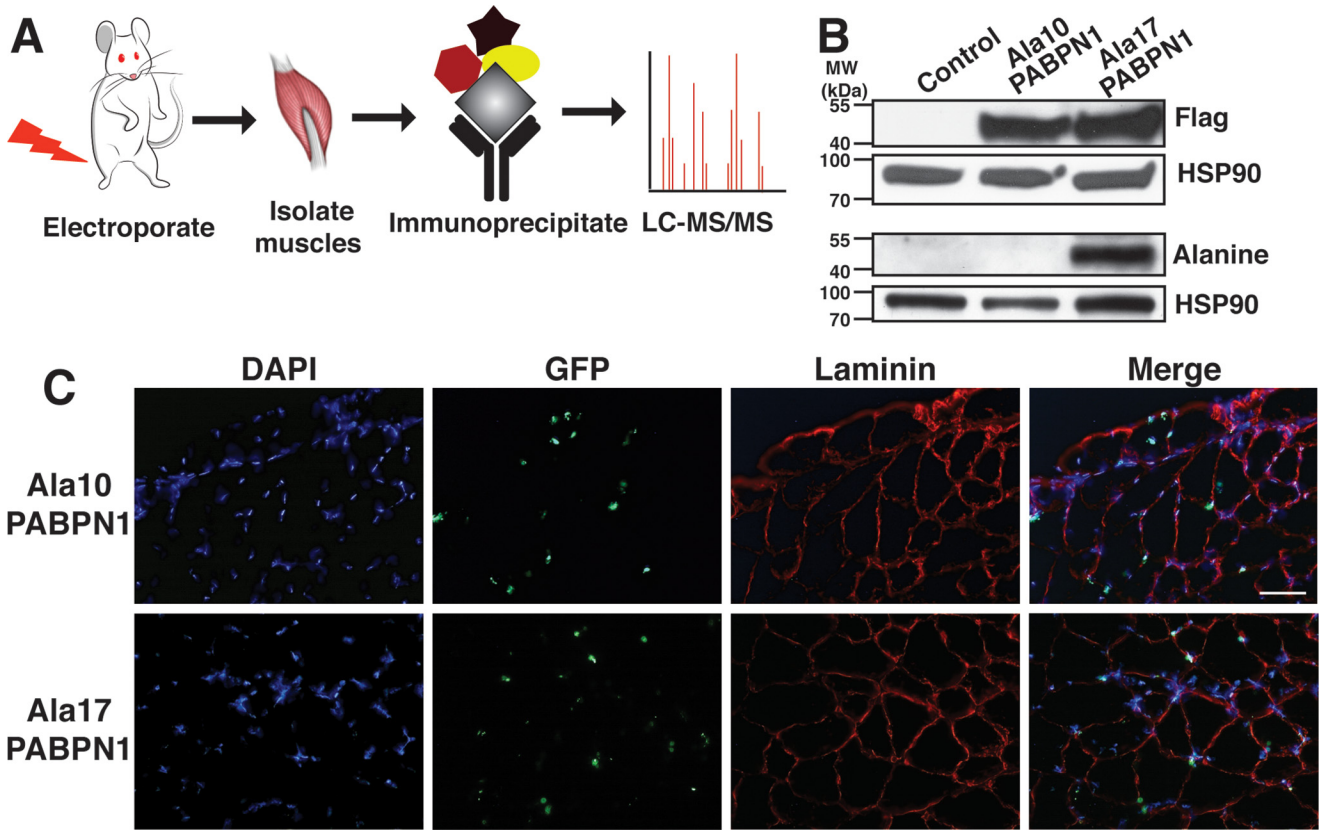

Figure 1. WT (Ala-10) and alanine-expanded (Ala-17) PABPN1 are expressed and localized to the nucleus in electroporated skeletal muscle. *A*, a schematic outlining the experimental approach to identify proteins that associate with PABPN1. For each plasmid, $n = 2$ hind limb (tibialis anterior and gastrocnemius) muscles from two mice were analyzed. *B*, lysates from muscles electroporated with plasmids expressing FLAG-tagged WT (Ala-10) PABPN1 or alanine-expanded (Ala-17) PABPN1 or a control plasmid were resolved by SDS-PAGE and analyzed by immunoblotting with either an anti-FLAG antibody (*top two blots*) or using an antibody that specifically detects alanine-expanded PABPN1 (36) (*bottom two blots*). HSP90 serves as a loading control. Shown is a representative image from $n = 2$ immunoblots using lysate from four electroporated mice. *C*, limb muscle (gastrocnemius) was electroporated with plasmids expressing WT (Ala-10) GFP-PABPN1 or alanine-expanded (Ala-17) GFP-PABPN1. Muscles were collected and sectioned 6 days after electroporation and analyzed by microscopy for GFP localization to detect GFP-PABPN1. DAPI and laminin staining mark the nuclei and muscle basal lamina, respectively.

were detected only in the Ala-10 PABPN1 immunoprecipitation, whereas 129 proteins were found only in the Ala-17 PABPN1 immunoprecipitation (Table S1). These results reveal that more proteins interact with Ala-17 PABPN1 than Ala-10 PABPN1, which is consistent with the propensity for alanine-expanded PABPN1 to bind to other proteins with higher affinity than WT PABPN1 (27).

Gene Ontology (GO) analysis was performed on the three groups of proteins: those that immunoprecipitated similarly with both Ala-10 and Ala-17 PABPN1 (Fig. 2*B*); those that immunoprecipitated preferentially with Ala-10 PABPN1 (Fig. 2*C*); and those that immunoprecipitated preferentially with Ala-17 PABPN1 (Fig. 2*D*). Interacting proteins were grouped based on biological process, cellular component, and molecular function with respect to *Z* score. Regulation of RNA stability and mRNA processing are two of the top biological processes identified for the proteins interacting equally with Ala-10 and Ala-17 PABPN1, whereas regulation of transcription and regulation of RNA stability are the top biological processes for proteins interacting more with Ala-10 and Ala-17 PABPN1, respectively. Several proteins previously identified as PABPN1 interactors including PABPC1, MATR3, and SKIP/SNW (28, 29) were identified in these immunoprecipitation experiments. The identification of known interactors and of other regulators of RNA metabolism provides further confidence in the validity of this proteomic analysis.

The co-precipitating proteins that belong to each GO term for Ala-10 PABPN1 interactors (Ala-10 > Ala-17) (Fig. 2*C*) or Ala-17 PABPN1 interactors (Ala-17 > Ala-10) (Fig. 2*D*) are shown in Fig. 3, *panel A* (Ala-10 PABPN1) and *panel B* (Ala-17 PABPN1) as *circular graphs*, with the colors representing the GO categories and the names of the proteins listed around the circumference. Of the 49 proteins that immunoprecipitated preferentially with Ala-10 PABPN1, SKIP/SNW (Fig. 3*A*), one is a transcriptional regulator important for skeletal muscle differentiation and is a known interactor of PABPN1 (28). The proteins identified that interact preferentially with alanine-expanded PABPN1 are more numerous and include MATR3 (Fig. 3*B*), which was recently characterized as a PABPN1 interactor in skeletal muscle (29). Numerous RNA-binding proteins including hnRNPC, hnRNPM, ELAVL1, TDP-43, and the RNA helicases DHX9 and DDX39B also preferentially immunoprecipitated with alanine-expanded PABPN1.

To validate the MS results, we confirmed the interaction of PABPN1 with hnRNPUL2, which immunoprecipitated similarly with Ala-10 and Ala-17 PABPN1, as well as the previously reported interaction with SKIP/SNW1, which immunoprecipitated preferentially with Ala-10 PABPN1. An antibody specific

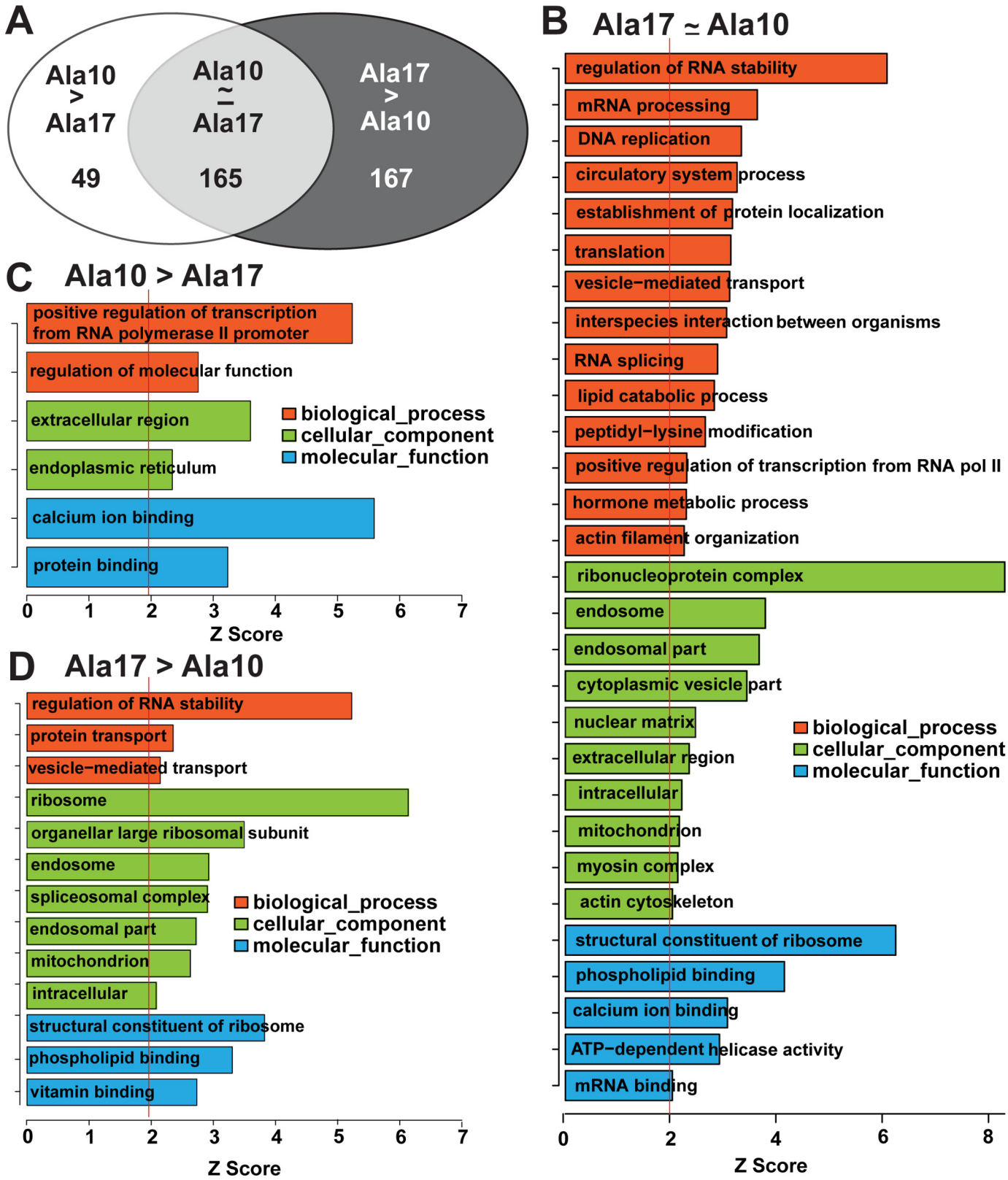

Figure 2. GO term analysis of protein–protein interactions of WT and expanded PABPN1. *A*, Venn diagram showing the number of proteins that interact with WT (Ala-10) PABPN1 and alanine-expanded (Ala-17) PABPN1. The number of proteins that interact to the same extent with Ala 10 and Ala-17 PABPN1 (Ala-10 ≈ Ala-17), more with Ala-10 than Ala-17 PABPN1 (Ala-10 > Ala-17), and more with Ala-17 than Ala-10 PABPN1 (Ala-17 > Ala-10) are indicated. *B–D*, the GO terms for the proteins that are equally enriched with WT (Ala-10) PABPN1 and alanine-expanded (Ala-17) PABPN1 (Ala-10 ≈ Ala-17, *B*) as compared with an IgG control or preferentially enriched with Ala-10 (Ala-10 > Ala-17, *C*) or Ala-17 (Ala-17 > Ala-10, *D*) PABPN1 are shown. Inclusion criteria for this analysis are *Z* score ≥ 2.0, *p* value < 0.00001, and ≥5 genes per GO term.

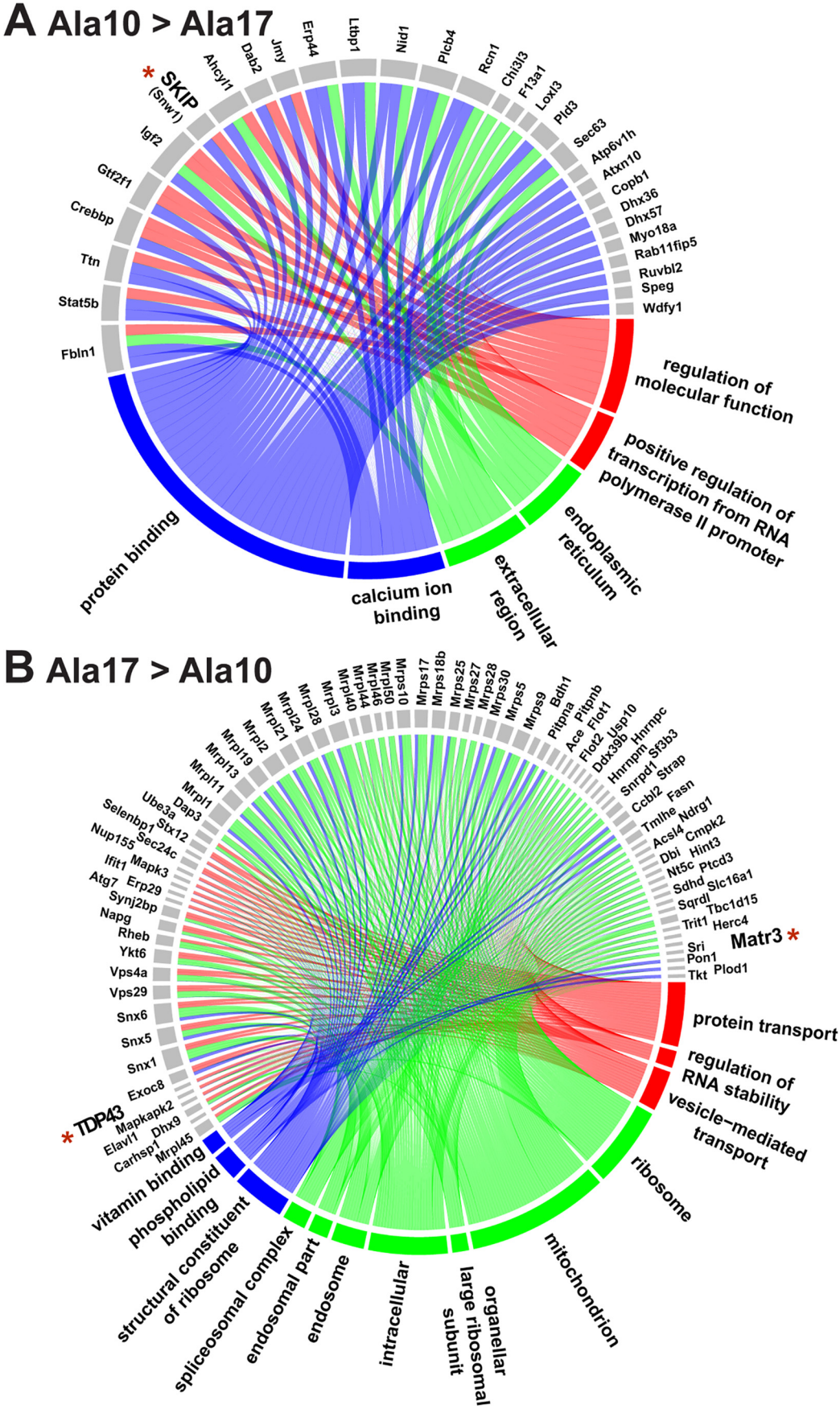
A Ala10 > Ala17
Erp44
Ltbp1
Nid1
Plcb4
Rcn1
Chi3l3
F13a1
Loxl3
Pld3
Sec63
Atp6v1h
Atxn10
Copb1
Dhx36
Dhx57
Myo18a
Rab11fip5
Ruvbl2
Speg
Wdfy1
regulation of molecular function
positive regulation of transcription from RNA polymerase II promoter
endoplasmic reticulum
extracellular region
calcium ion binding
protein binding
Fbln1
Stat5b
Ttn
Crebbp
Gtf2f1
Igf2
* SKIP (Snw1)
Ahcyl1
Dab2
Jmy
B Ala17 > Ala10
Mrps10
Mrps17
Mrps18b
Mrps25
Mrps27
Mrps28
Mrps30
Mrps5
Mrps9
Bdh1
Pitpna
Pitpnb
Ace
Flot1
Flot2
Usp10
Ddx39b
Hnrnpc
Hnrnpm
Sf3b3
Snrpd1
Strap
Ccbl2
Fasn
Tmlhe
Ndrg1
Acsl4
Cmpk2
Dbi
Hint3
Nt5c
Ptcd3
Sdhd
Slc16a1
Sqrdl
Tbc1d15
Trit1
Herc4
Sri
Matr3 *
Pon1
Tkt
Plod1
protein transport
regulation of RNA stability
vesicle−mediated transport
ribosome
mitochondrion
organellar large ribosomal subunit
intracellular
endosome
endosomal part
spliceosomal complex
structural constituent of ribosome
phospholipid binding
vitamin binding
* TDP43
Mrpl45
Carhsp1
Elavl1
Dhx9
Mapkapk2
Exoc8
Snx1
Snx5
Snx6
Vps29
Vps4a
Ykt6
Rheb
Napg
Synj2bp
Atg7
Erp29
Ifit1
Mapk3
Nup155
Sec24c
Selenbp1
Stx12
Ube3a
Dap3
Mrpl1
Mrpl11
Mrpl13
Mrpl19
Mrpl2
Mrpl21
Mrpl24
Mrpl28
Mrpl3
Mrpl40
Mrpl44
Mrpl46
Mrpl50

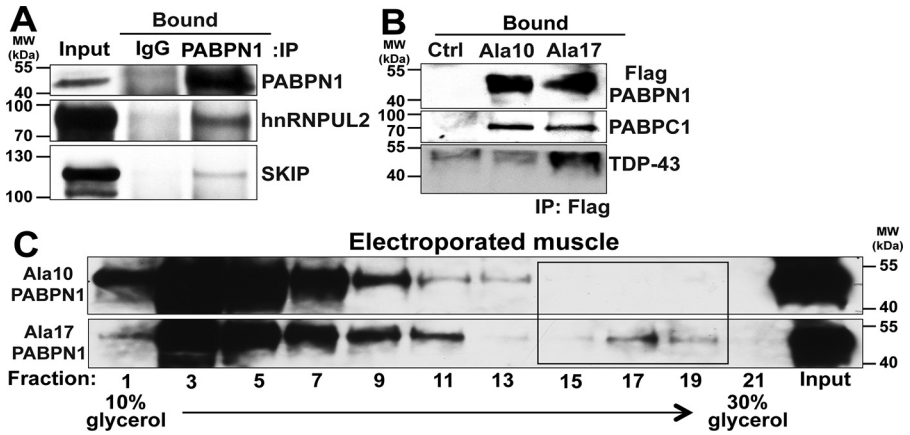

Figure 4. Protein interactions of WT (Ala-10) PABPN1 and alanine-expanded (Ala-17) PABPN1. *A*, to examine interaction with endogenous PABPN1, skeletal muscle (gastrocnemius) lysate was incubated with control IgG or an antibody against PABPN1 (22). Input and bound fractions were resolved by SDS-PAGE and immunoblotted with anti-PABPN1, anti-hnRNPUL2, or anti-SKIP/SNW antibody. Shown is a representative image from $n = 2$ immunoblots using lysate from four electroporated mice. *B*, to examine differential interactions with WT and alanine-expanded PABPN1, lysates obtained from muscles electroporated with plasmids expressing WT (Ala-10) or alanine-expanded (Ala-17) PABPN1 were incubated with anti-FLAG antibody conjugated beads. Bound fractions were resolved by SDS-PAGE followed by immunoblotting with anti-FLAG, anti-PABPC1, and anti–TDP-43 antibodies. Shown is a representative image from $n = 2$ immunoblots using lysate from four electroporated mice. *C*, lysates obtained from muscles electroporated with plasmids expressing FLAG-tagged WT (Ala-10) or alanine-expanded (Ala-17) PABPN1 were analyzed by sedimentation through 10–30% glycerol gradients. Alternate gradient fractions from *top* to *bottom* were loaded from *left* to *right* together with an input lane and resolved by SDS-PAGE. Immunoblotting with an anti-FLAG antibody was used to detect WT (Ala-10) PABPN1 or alanine-expanded (Ala-17) PABPN1 in the fractions. Shown is a representative immunoblot from three separate fractionation experiments. The *box* highlights Ala-17 PABPN1 present in high-molecular-weight complexes.

for PABPN1 (22) or control IgG was used to perform immunoprecipitations from control mouse muscle lysates that express only endogenous PABPN1. Immunoblot analysis of input and bound samples demonstrates that both hnRNPUL2 and SKIP/SNW immunoprecipitate with endogenous PABPN1 from skeletal muscle lysate (Fig. 4*A*).

To validate differential interactions with Ala-10 and Ala-17 PABPN1, WT and alanine-expanded FLAG-tagged PABPN1 were immunoprecipitated from electroporated skeletal muscle lysate using FLAG antibody. Immunoblot analysis with FLAG antibody shows that equal amounts of Ala-10 and Ala-17 PABPN1 are immunoprecipitated from the muscle lysate (Fig. 4*B*). The bound samples were then immunoblotted for PABPC1, which immunoprecipitated equally with Ala-10 and Ala-17 PABPN1, and TDP-43, which immunoprecipitated only with Ala-17 PABPN1 (Fig. 3). Immunoblot analysis shown in Fig. 4*B* confirms that PABPC1 interacts similarly with both Ala-10 and Ala-17 PABPN1, whereas TDP-43 is enriched only in the immunoprecipitation of Ala-17 PABPN1. These results are consistent with results obtained from mass spectrometric analysis that revealed differential interactions between Ala-10 and Ala-17 PABPN1.

Most previous studies have focused on proteins that interact with alanine-expanded PABPN1 in the context of intranuclear aggregates (13, 14, 27). The studies described here were performed utilizing only soluble cellular fractions, so identified Ala-17 PABPN1 interactions do not represent aggregated proteins. However, they may be components of higher-molecular-weight complexes. To assess whether Ala-17 PABPN1 exists in larger protein complexes than Ala-10 PABPN1, lysates from electroporated muscles were resolved on a density gradient followed by immunoblotting for FLAG-tagged PABPN1. As shown in Fig. 4*C*, Ala-17 PABPN1 migrates in heavier fractions than Ala-10 PABPN1, which is consistent with the finding that Ala-17 PABPN1 interacts with multiple proteins and thus can form complexes with higher molecular weights than Ala-10 PABPN1.

TDP-43 is present in high-molecular-weight complexes that contain alanine-expanded PABPN1

To better understand how aberrant protein interactions with Ala-17 PABPN1 may be linked to pathology, we sought to further characterize the interaction between Ala-17 PABPN1 and TDP-43, which immunoprecipitated only with Ala-17 PABPN1 (Figs. 3*B* and 4*B*). TDP-43 is an RNA-binding protein that is linked to the pathogenesis of ALS and myopathies, which is prone to aggregate formation in the context of neuromuscular disease (39–41). Furthermore, recent work shows that TDP-43 plays a critical role in muscle formation and forms amyloid-like structures during myogenesis (32). Given that Ala-17 PABPN1 forms high-molecular-weight complexes as shown by altered migration on a glycerol gradient (Fig. 4*C*), we performed a series of experiments to examine the characteristics of TDP-43 in the presence of Ala-17 PABPN1.

To assess the solubility of TDP-43 in the presence of Ala-17 PABPN1, we exploited a recently published knock-in mouse model of OPMD (33). These mice genocopy OPMD patients with one allele encoding Ala-10 PABPN1 and one encoding Ala-17 PABPN1 under the control of the native *Pabpn1* promoter. As with a number of RNA-binding proteins, the levels of

Figure 3. Circular diagrams of the differential interactions of WT PABPN1 (Ala-10) and alanine-expanded (Ala-17) PABPN1. The genes that cluster into the listed GO terms in Fig. 2 that are specific for proteins that preferentially interact with WT PABPN1 (Ala-10 > Ala-17, *A*) or alanine-expanded PABPN1 (Ala-17 > Ala-10, *B*) are depicted. The corresponding GO terms are shown by a connecting line in the color corresponding to the GO term: *red*, biological process; *green*, cellular component; and *blue*, molecular function. Previously identified protein interactors of PABPN1 are shown in *bold* and indicated by the *red asterisks*.

TDP-43 are low in mature muscle but are increased in isolated primary myoblasts (42), which can be differentiated into myotubes *in vitro* (43). Thus, we examined TDP-43 in both primary myoblasts and myotubes prepared from control WT Ala-10/Ala-10 PABPN1 mice and the OPMD model Ala-17/Ala-10 PABPN1 mice.

Primary myoblasts isolated from WT mice (Ala-10/Ala-10) or OPMD mice (Ala-17/Ala-10) were differentiated into myotubes and lysed in a gentle lysis buffer followed by centrifugation. Immunoblot analysis of the soluble and pellet fractions shows that more TDP-43 is present in the pellet fraction obtained from myotubes of the OPMD model (Ala-17/Ala-10) as compared with pellet fraction obtained from WT myotubes (Ala-10/Ala-10) (Fig. 5*A*). The soluble fractions from WT and OPMD model myotubes were also loaded and resolved on 10–30% glycerol density gradients. Immunoblot analysis of fractions collected from top to bottom of the density gradients shows that TDP-43 in lysate from OPMD model (Ala-17/Ala-10) myotubes migrates in heavier fractions when compared with lysate prepared from WT (Ala-10/Ala-10) myoblasts (Fig. 5*B*). These results imply that soluble TDP-43 exists in larger protein complexes in myotubes expressing Ala-17 PABPN1 than in control myotubes.

TDP-43 is regulated by redox-mediated cysteine oxidation that results in high-molecular-weight (HMW) species, which are prone to aggregation (44). Given the mitochondrial dysfunction found in the OPMD mouse model (33), the presence of TDP-43 in pellet fractions may be related to redox-mediated aggregation. To determine whether TDP-43 is more susceptible to redox-mediated aggregation in cells that express Ala-17 PABPN1 compared with control, myoblasts from OPMD Ala-17/Ala-10 and WT Ala-10/Ala-10 mice were treated with hydrogen peroxide (+) or left untreated (−) prior to lysis in the absence of reducing agents. As shown in Fig. 5*C*, immunoblot analysis reveals that there is HMW TDP-43 in the pellet fraction from Ala-17 PABPN-expressing cells prior to treatment with hydrogen peroxide (−). After treatment with hydrogen peroxide, even more HMW TDP-43 was detected in the pellet fraction from OPMD model cells expressing Ala-17 PABPN1. HMW TDP-43 was not detected in the pellet fraction in control cells that express Ala-10/Ala-10 PABPN1 in either the absence (−) or the presence (+) of hydrogen peroxide treatment. This result demonstrates that TDP-43 is more prone to redox-mediated aggregation in cells obtained from the OPMD Ala-17/Ala-10 mouse model compared with WT muscle cells.

The presence of TDP-43 in HMW species in primary muscle cells isolated from an OPMD Ala-17/Ala-10 mouse model could suggest that TDP-43 is present in PABPN1-containing intranuclear aggregates associated with OPMD. To determine whether TDP-43 associates with PABPN1 Ala-17 aggregates, we employed a transgenic Ala-17–overexpressing mouse model of OPMD (Ala-17.1), in which PABPN1 forms readily detectable aggregates in skeletal muscle (34). These aggregates are functionally defined as KCl-insoluble and are thus detectable after KCl washout of soluble proteins (7). Muscle sections obtained from WT mice or the Ala-17 PABPN1-overexpressing mice (Ala-17.1) were treated with salt (+KCl) to wash away soluble proteins and reveal aggregates or left untreated (−KCl) and then immunostained using an antibody to detect TDP-43. Immunofluorescence staining reveals nuclear TDP-43 staining in the KCl-treated muscle sections (Fig. 5*D*), indicating that TDP-43 can accumulate in nuclear aggregates that occur in muscle overexpressing alanine-expanded PABPN1.

TDP-43 protein dysfunction in OPMD model cells

The presence of TDP-43 in higher-molecular-weight and insoluble complexes may render it unavailable to perform normal functions related to RNA splicing. To assess whether TDP-43 interaction with Ala-17 PABPN1 impairs TDP-43 function, we evaluated the alternative splicing of known TDP-43 RNA targets (45–48). If TDP-43 function is impaired by association with alanine-expanded PABPN1, these alternative splicing events might show changes comparable with the loss of TDP-43 function. For this analysis, RNA from WT Ala-10/Ala-10 and OPMD Ala-17/Ala-10 myoblasts was reverse-transcribed into cDNA, followed by RT-PCR to detect alternative splicing of the previously characterized TDP-43 targets *Mef2D*, *Sort1*, and *Dnajc5* (45–47). As shown in Fig. 6 (*A* and *B*), we detect increased inclusion of cassette exons in the *Mef2D* (exon 8) and *Sort1* (exon 17b) transcripts but not *Dnajc5* (exon 4) in myoblasts obtained from the OPMD Ala-17/Ala-10 mouse model as compared with WT Ala-10/Ala-10 myoblasts. Exon inclusion in *Sort1* was also quantified using quantitative RT-PCR with primers specific for the exon 17b–included and exon 17b–excluded transcripts. Results from quantitative RT-PCR analysis confirm the increased inclusion of the *Sort1* 17b cassette exon in myoblasts isolated from the OPMD Ala-17/Ala-10 mouse model (Fig. 6*C*). These data suggest that TDP-43 function is impaired in muscle cells expressing Ala-17 PABPN1.

To extend this analysis of the consequences of TDP-43 high-molecular-weight complex formation in Ala-17 PABPN1-expressing cells, we sought to understand the functional implications of altered *Sort1* splicing. SORT1 is a sorting receptor expressed on the cell surface, endoplasmic reticulum, and Golgi apparatus, which is involved in the transport of a wide variety of proteins including the glucose transporter GLUT4 and progranulin (PGRN) (49–52). TDP-43 represses the inclusion of *Sort1* exon 17b, suggesting that SORT1 function could be dysregulated under conditions where functional levels of TDP-43 are decreased.

To assess SORT1 function, we analyzed uptake of both glucose (50) and PGRN (51, 52) into WT Ala-10/Ala-10 and OPMD Ala-17/Ala-10 myoblasts and myotubes. SORT1 regulates GLUT4 (50), which modulates cellular glucose uptake (53). Glucose uptake was measured by incubating myoblasts or myotubes with the fluorescent glucose analog 2-(*N*-(7-nitrobenz-2-oxa-1,3-diazol-4-yl)amino)-2-deoxyglucose (2-NBDG). As shown in Fig. 7*A*, both myoblasts and myotubes from OPMD Ala-17/Ala-10 mice show increased intracellular fluorescence, indicating increased uptake of 2-NBDG and suggesting an increased capacity for glucose uptake. To measure PGRN uptake, cultured WT Ala-10/Ala-10 and OPMD Ala-17/Ala-10 myotubes were incubated overnight with N-terminally TAP-tagged recombinant human progranulin (N-TAP PGRN) (54). Immunoblot analysis to detect intracellular PGRN as a measure of PGRN uptake revealed that N-TAP PGRN accumulation is

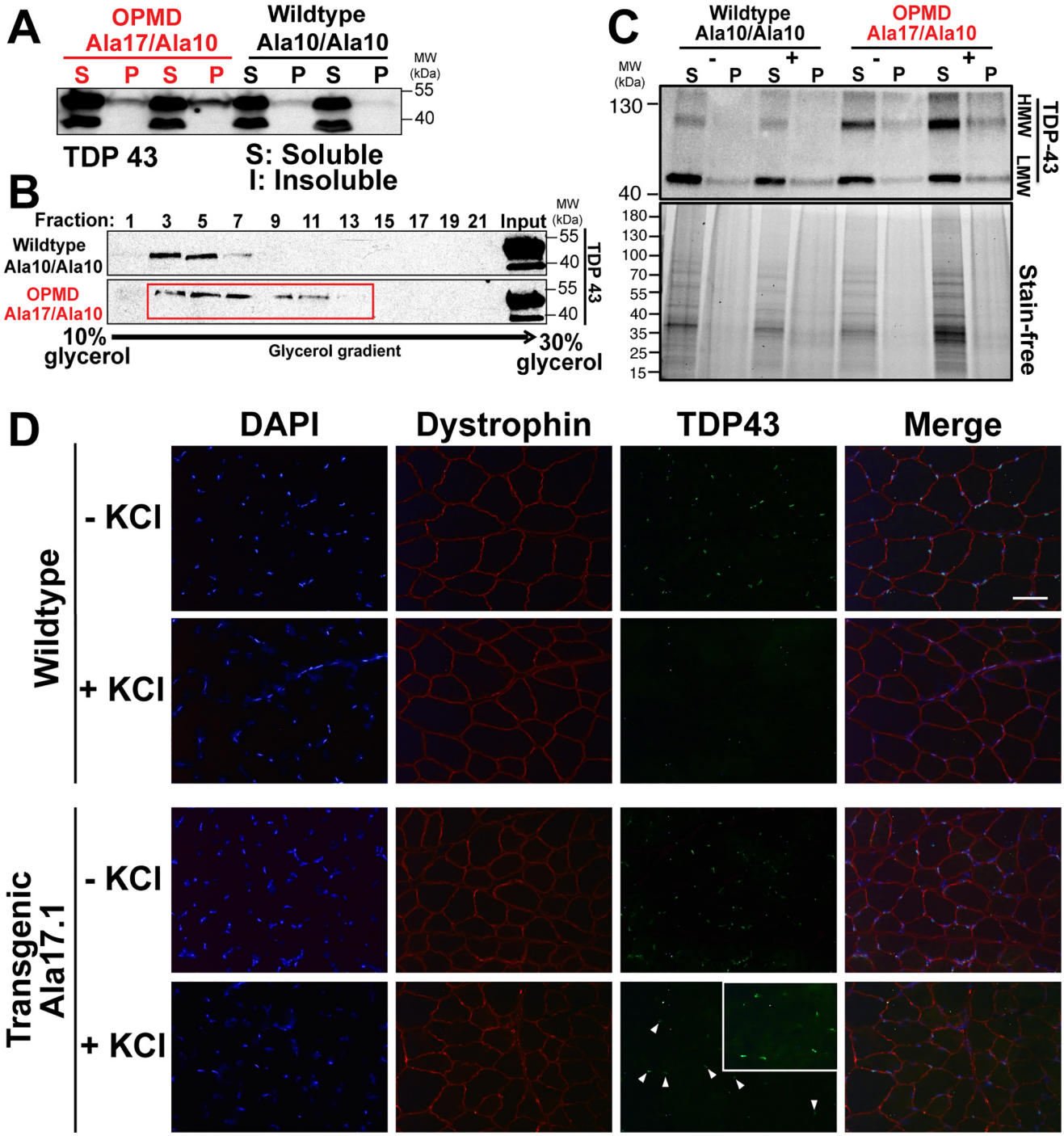

Figure 5. TDP-43 protein physiology is altered in myoblasts expressing Ala-17 PABPN1. *A*, primary myoblasts isolated from WT (Ala-10/Ala-10) or OPMD model (Ala-17/Ala-10) mice were differentiated into myotubes and lysed in a gentle lysis buffer. The soluble (*S*) and pellet (*P*) fractions following centrifugation were resolved by SDS-PAGE and immunoblotted to detect TDP-43. The *top* and *bottom bands* represent TDP-43 full-length and 35-kDa cleavage product, respectively (90). Shown is a representative immunoblot for three independent experiments. *B*, soluble lysates obtained from WT (Ala-10/Ala-10) or OPMD (Ala-17/Ala-10) myotubes prepared in *A* were resolved on density glycerol gradients, and fractions were collected from *top* to *bottom*. Input samples and alternate fractions were resolved by SDS-PAGE and immunoblotted for TDP-43. Shown is a representative immunoblot for three independent experiments. *C*, myoblasts isolated from WT (Ala-10/Ala-10) and OPMD (Ala-17/Ala-10) mice were cultured in the absence (−) or presence (+) of 1 mM hydrogen peroxide followed by lysis in a nonreducing buffer (−DTT). Lysates were resolved by SDS-PAGE and immunoblotted for TDP-43 to detect low-molecular-weight (*LMW*) and HMW species of TDP-43. Shown is a representative immunoblot for three independent experiments. *D*, limb muscles from WT and transgenic Ala 17.1 mice (34) were sectioned and permeabilized. Sections were left untreated (−KCl) or treated with 1 M KCl in HPEM buffer (+KCl) to remove soluble proteins, followed by detection of TDP-43 with anti–TDP-43 antibody. KCl-insoluble aggregates are indicated by *white arrowheads* and are magnified in the *inset*. DAPI and dystrophin staining were used to mark the nucleus and sarcolemma, respectively.

significantly increased in OPMD myotubes when compared with WT myotubes (Fig. 7, *B* and *C*). As a control, myotubes were also incubated with C-terminal TAP-tagged progranulin (C-TAP PGRN), which does not interact with SORT1 and should therefore not be imported (55). The absence of C-TAP PGRN uptake into either WT or OPMD myotubes provides

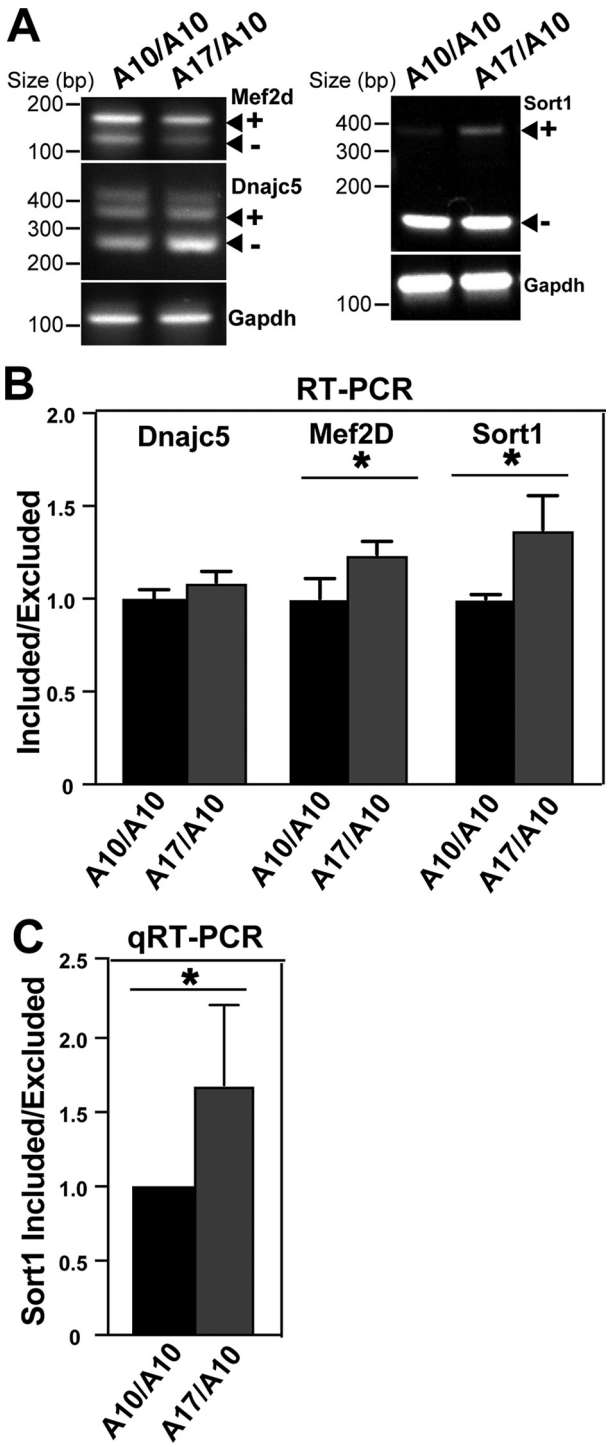

Figure 6. TDP-43 regulated alternative splicing is altered in cells expressing alanine-expanded PABPN1. *A*, analysis of RT-PCR products of alternatively spliced exons of *Mef2D* (exon 8), *Sort1* (exon 17b), and *Dnajc5* (exon 4) using RNA isolated from WT Ala-10/Ala-10 (A10/A10) or OPMD Ala-17/Ala-10 (A17/A10) primary mouse myoblasts. *Gapdh* serves as a loading control. The *upper* and *lower bands* are the exon-included (+) and exon-excluded (−) PCR products, respectively. *B*, densitometric quantification of the exon-included and exon-excluded RT-PCR products from *A* is presented as a ratio of included/excluded PCR products. Shown is mean plus or minus standard deviation for $n = 3$; * indicates $p < 0.05$. *C*, quantitative RT-PCR analysis of *Sort1* alternative splicing in WT (A10/A10) or OPMD (A17/A10) primary mouse myoblasts. The steady-state level of *Sort1* RNA with exon 17b included or excluded was quantified by quantitative (q)RT-PCR using variant-specific primers and is represented as the *Sort1* included/excluded ratio normalized to *Gapdh*. The data shown represent mean plus or minus standard deviation for $n = 16$. * indicates $p < 0.05$.

evidence that SORT1-mediated import is responsible for enhanced uptake of N-TAP PGRN in OPMD Ala-17/Ala-10 myotubes (Fig. 7*D*). The increased uptake of both glucose and N-TAP PGRN suggests that the inclusion of the cassette exon in *Sort1* affects the function of the SORT1 protein in muscle cells that express Ala-17 PABPN1.

Discussion

Characterizing and comparing the protein–protein interactions of Ala-10 and Ala-17 PABPN1 in muscle is critical to understand the various functions of PABPN1 while identifying pathways most susceptible to dysfunction. Ideally, affinity purification of endogenous WT or alanine-expanded PABPN1 from skeletal muscle followed by MS would identify the co-immunoprecipitating protein interactors of PABPN1. However, existing disease models of OPMD either have variable degrees of overexpression of the WT and alanine-expanded proteins (34) or express low endogenous levels of PABPN1 in skeletal muscle (15, 33), which hinders such a proteomics approach. To circumvent these technical challenges, we exploited several different mouse models. To achieve comparable expression of WT and alanine-expanded PABPN1, we employed electroporated mouse skeletal muscles with plasmids expressing similar levels of FLAG-tagged Ala-10 or Ala-17 PABPN1. Immunoprecipitation of FLAG-PABPN1 from these electroporated muscles followed by MS allowed for the first comparison of the protein interactions of the WT and OPMD-associated alanine-expanded PABPN1 in skeletal muscle tissue. We then used several additional mouse models and experimental conditions to validate and explore the functional consequences of the interactions identified. We validated interactions with WT PABPN1 using control mouse skeletal muscle (Fig. 4*A*). We also examined the possible consequences of TDP-43 interactions with alanine-expanded PABPN1 by employing two additional OPMD mouse models. To assess whether TDP-43 is detected in aggregates in an OPMD mouse model, we used a transgenic mouse model (Ala-17.1 PABPN1 (34)) that overexpresses Ala-17 PABPN1 in skeletal muscle (Fig. 5*D*). This model was employed for this experiment because insoluble aggregates are readily detectable (34). We extended our analysis of TDP-43 function to a mouse model where alanine-expanded PABPN1 is expressed from the endogenous *Pabpn1* locus (33). This model genocopies OPMD patients who have one WT and one mutant allele of *PABPN1*. This model was selected because it most closely reflects the situation that would occur in muscle tissue from individuals with OPMD. Thus, each model was carefully selected to provide insight into the PABPN1 protein–protein interactions in skeletal muscle as well as to identify potential functional consequences that could occur when alanine-expanded PABPN1 is expressed in disease.

Co-immunoprecipitation followed by MS identified three discrete groups of PABPN1 protein interactors. The first group immunoprecipitated equally with Ala-10 and Ala-17 PABPN1, whereas the second showed preferential interaction with Ala-10 PABPN1 and potentially represents proteins that the OPMD-associated Ala-17 PABPN1 cannot access. The third group of proteins was much larger and showed preferential interaction with Ala-17. For the group of proteins that interacts

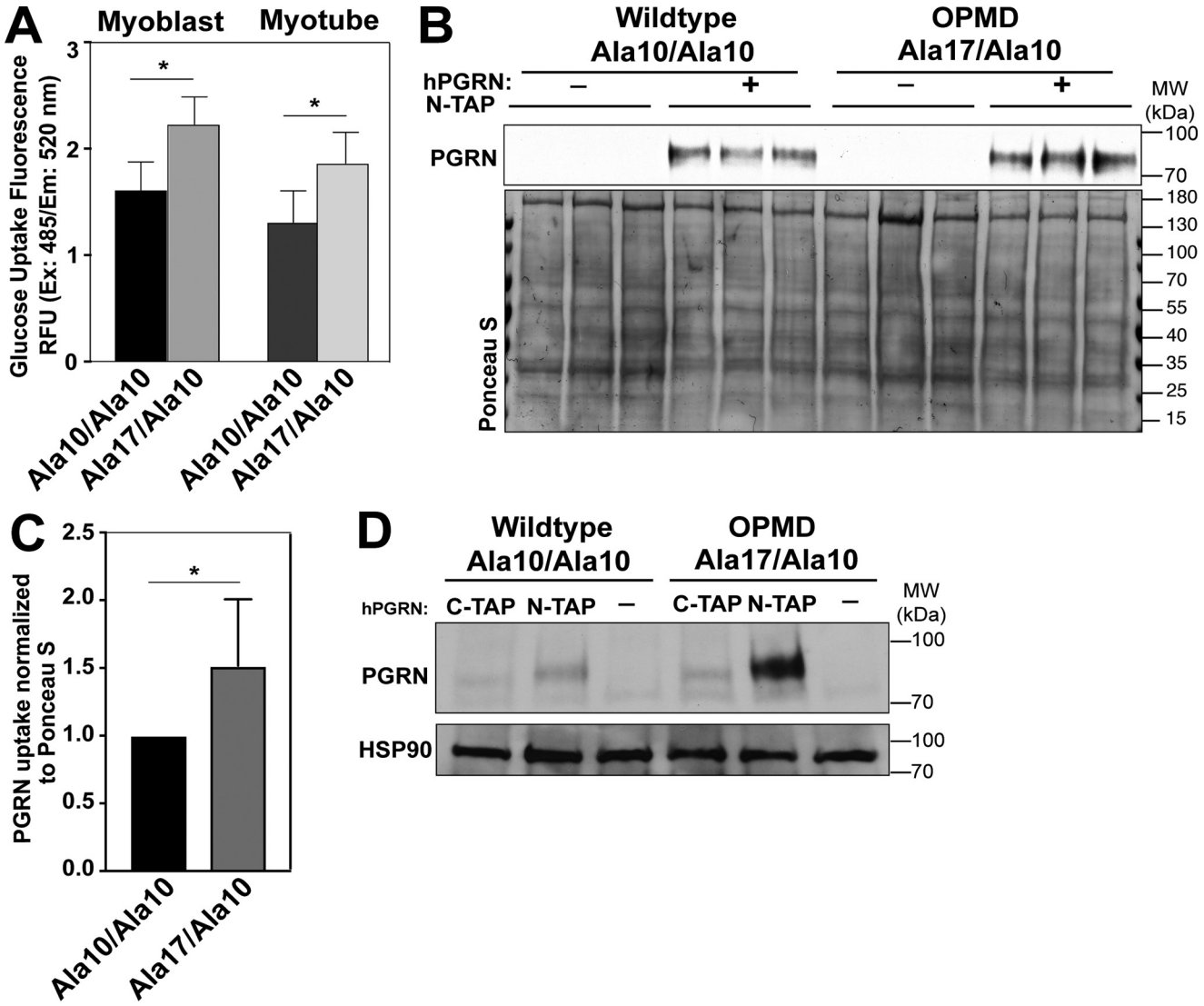

Figure 7. SORT1 protein function is altered in muscle cells that express alanine-expanded PABPN1. *A*, WT (Ala-10/Ala-10) and OPMD (Ala-17/Ala-10) myoblasts and myotubes were cultured in the presence of a fluorescent glucose analog 2-NBDG for 6 h. Cellular fluorescence (RFU) was measured with a plate reader as a reporter for glucose uptake. Shown is mean plus or minus standard deviation for $n = 3$ experiments. * indicates $p < 0.05$. *B*, WT (Ala-10/Ala-10) and OPMD (Ala-17/Ala-10) myotubes were cultured in the presence or absence of recombinant N-TAP human progranulin (PGRN) for 16 h. Cell lysates were resolved by SDS-PAGE followed by immunoblotting for PGRN for three independent samples for each condition analyzed. *C*, band intensities for PGRN uptake from *B* were quantified and normalized to total protein (Ponceau S staining). Shown is mean plus or minus standard deviation for $n = 4$ experiments. * indicates $p < 0.05$. *D*, to control for the specificity of PGRN uptake, WT (Ala-10/Ala-10) and OPMD (Ala-17/Ala-10) myotubes were cultured in the presence or absence of recombinant N-terminally TAP-tagged (N-TAP) or C-terminally TAP-tagged (C-TAP) human PGRN for 16 h. Cell lysates were resolved by SDS-PAGE followed by immunoblotting for PGRN. HSP90 serves as a loading control.

similarly with WT and alanine-expanded PABPN1, we cannot rule out the possibility that some of these interactions could be RNA-mediated. However, we employed conditions for the immunoprecipitation where we have not detected a difference upon RNase treatment (29).

The increased number of proteins that immunoprecipitate with Ala-17 PABPN1 is consistent with model that alanine expansion increases the affinity of PABPN1 for other proteins (56). Given that immunoprecipitations were performed on soluble lysate from muscle tissue expressing Ala-17 PABPN1, the increased protein interactions with Ala-17 PABPN1 do not represent the intranuclear aggregates detected in the muscles of individuals with OPMD and OPMD mouse models. However, these interactions may represent high-molecular-weight complexes that could seed the formation of PABPN1-containing aggregates. Therefore, the proteins that immunoprecipitated preferentially with Ala-17 PABPN1 could be most susceptible to sequestration in OPMD-associated aggregates. Indeed, a previously published study suggested the formation of preinclusion-like structures in cells expressing alanine-expanded PABPN1, but the study did not report the components of these structures or the mechanistic implications of their formation (57).

The proteins that interact equally with both Ala-10 and Ala-17 PABPN1 include poly(A)-binding proteins (PABPC1, PABPC4, and PAIP1), hnRNPs (HNRNPUL2, Q, and H1/H2), and other critical RNA-binding proteins, including EIF4A, AUF1, and NPM1. In addition to RNA-binding proteins, the methyltransferase PRMT1 was also identified as a PABPN1 interactor. We previously identified PABPC1, PABPC4, and

HNRNPQ as protein interactors of PABPN1 in skeletal muscle (29). Furthermore, previous reports demonstrated that PABPN1 interacts with arginine methyltransferases (27, 56), and arginine methylation regulates PABPN1 function (58). The identification of established interactors in these proteomic data sets provides validation to support the novel protein interactions identified. These newly identified PABPN1 protein interactors could not only provide insight into the currently known functions of PABPN1 but also uncover new functions of PABPN1 in muscle cells.

The largest group of PABPN1 interactors includes proteins that interact preferentially with the OPMD-associated Ala-17 PABPN1. The interactors of Ala-17 PABPN1 fall under a wide range of functional and biological classifications and could represent aberrant protein–protein interactions with the alanine-expanded PABPN1. These proteins and the cellular processes they regulate could be most susceptible to loss of function caused by sequestration in high-molecular-weight complexes or intranuclear aggregates in OPMD. Alternatively, they could mediate some deleterious gained function when in complex with alanine-expanded PABPN1. The Ala-17 PABPN1 interactors include numerous proteins that are involved in post-transcriptional regulation of RNA including DHX9 (59), CSDE1 (60), ELAVL1 (HuR) (61, 62), and RENT1 (63, 64). DHX9 is a nuclear RNA helicase that processes dsRNA and circular RNA (59, 65). DHX9 also associates with proteins such as FUS, which is linked to aggregation in amyotrophic lateral sclerosis (ALS) (66, 67). We also detected a number of mitochondrial ribosomal proteins that preferentially interact with Ala-17 PABPN1. Given the high abundance of mitochondrial ribosomal proteins in skeletal muscle, these proteins are often considered contaminants in immunoprecipitation experiments. However, mitochondrial dysfunction has been detected in patient tissues and animal models of OPMD and other repeat expansion disorders (33, 68–70). Polyalanine stretches directly associate with mitochondrial proteins in mouse brain and muscle lysate (71) and are associated with apoptosis resulting from mitochondrial dysfunction (72). Additionally, dipeptide repeats expressed from *C9ORF72* repeat expansions associate with mitochondrial ribosome subunits and compromise mitochondrial function (73). In addition to these expanded proteins, mutations in genes encoding other disease-linked proteins such as TDP-43 are also associated with aberrant mitochondrial localization of mutant proteins and mitochondrial dysfunction (74, 75).

Among the proteins identified to interact more with Ala-17 PABPN1 is the ALS-associated protein TDP-43 (76, 77), which interacts with PABPN1 in mammalian cells (31, 78). TDP-43 was recently identified as a component of amyloid-like myo-granules that are localized near the sarcomeres in the cytosol of nascent myotubes in culture and myofibers *in vivo* (32). These myo-granules contain TDP-43 bound to mRNAs encoding critical myogenic factors including embryonic myosin heavy chain, thus highlighting the importance of TDP-43 in skeletal muscle formation. We detected soluble TDP-43 in high-molecular-weight fractions in glycerol gradient fractionation experiments and insoluble TDP-43 in muscle cells expressing Ala-17 PABPN1. These high-molecular-weight complexes may represent increased formation or persistence of myo-granules in Ala-17 PABPN1-expressing cells, early formation of insoluble nuclear TDP-43 aggregates that have been detected in mice overexpressing Ala-17 PABPN1, or an alternative high-molecular-weight complex. However, any of these scenarios have the potential to sequester TDP-43 and impair its normal functions. Indeed, we detected altered splicing of the known TDP-43 targets *Mef2d* and *Sort1*. The changes we detected in both *Sort1* and *Mef2D* splicing are comparable with changes that are detected when TDP-43 is depleted by siRNA (45, 48), supporting the idea that TDP-43 function is decreased in muscle cells that express alanine-expanded PABPN1.

TDP-43 binds a large complement of coding and noncoding RNAs (45, 79) and is a common component of aggregates in various neuromuscular diseases (30). TDP-43 interacts and aggregates with MATR3 (80, 81), which was identified as a PABPN1 interactor here and in our previous study (29). Furthermore, TDP-43 aggregation is found in skeletal muscles in some cases of sporadic and familial ALS (40), as well as in aggregates associated with inclusion body myositis and OPMD (30, 41, 82). Importantly, PABPN1 interacts with and ameliorates the toxicity of aggregation-prone TDP-43 variants in multiple model systems (31). In that study, expression of PABPN1 had minimal effect on endogenous TDP-43, but alanine-expanded PABPN1 was not tested. Our study suggests that alanine-expanded PABPN1 could have the opposite effect of WT PABPN1 by aberrantly binding to and sequestering functional TDP-43.

The group of proteins that interacts preferentially with Ala-10 PABPN1 when compared with Ala-17 PABPN1 includes proteins involved in transcription such as GTF2F1 (83), SAFB1 (84), and SKIP/SNW (85, 86). SAFB1 interacts with FUS (Fused-in-sarcoma) and MATR3, a PABPN1 interactor (29), to regulate splicing and transcription (87). SKIP/SNW interacts with PABPN1 to regulate expression of genes important for myogenesis (28). The identification of proteins that preferentially interact with WT PABPN1 suggests that alanine-expanded PABPN1 may not retain all of the functions of the WT protein. Thus, alanine expansion in PABPN1 can not only lead to a gain-of-function in the form of abnormal protein–protein contacts but also result in a loss-of-function by precluding critical protein interactions.

Although the role of protein aggregation in polyalanine and polyglutamine expansion disorders is widely accepted, it is unclear whether a loss or gain of protein function underlies disease pathogenesis. Pathology could arise from a combination of these effects, and the combined effects could be specific to certain tissues, providing some insight into the tissue specificity of disease. With respect to the different mechanisms, critical cellular proteins can be sequestered through specific or nonspecific interactions with aggregation prone disease-associated proteins such as PABPN1, leading to a loss of function. The aggregation prone proteins might also be unable to make appropriate protein interactions essential for their function. This study both identifies PABPN1-interacting proteins in muscle, a disease-relevant tissue, and sheds light on the complex mechanisms that can contribute to cellular dysfunction as a result of altered interactions with alanine-expanded protein.

Experimental procedures

Electroporation

All animals were housed and handled according Association for Assessment and Accreditation of Laboratory Animal Care guidelines and were approved by the Emory University Institutional Animal Care and Use Committee. Age- and sex-matched mice were anesthetized with an intraperitoneal injection of 91 mg/kg ketamine and 9.1 mg/kg xylazine. Tibialis anterior or gastrocnemius muscles were injected with 30 μl of 0.4 unit/microliter hyaluronidase solution in 0.9% NaCl with a 30-gauge needle. After 2 h, the mice were reanesthetized and injected with 30 μl of plasmid DNA (1 μg/microliter). The limbs to be electroporated were coated in ultrasound jelly and electroporated (ten 20-ms pulses of 175 V/cm with 480-ms intervals between pulses) using 7-mm platinum tweezer electrodes connected to an ECM 830 *in vivo* electroporator (BTX Harvard Apparatus). For each plasmid type, two animals were electroporated, and both tibialis anterior and gastrocnemius muscles were electroporated for each animal. The mice were euthanized 7 days following electroporation using a CO_2 chamber as per institutional animal care and use committee guidelines. Electroporated muscles were collected and flash frozen in cryofreezing medium (Sakura OCT-TissueTek) for sectioning with a cryostat (Leica Biosystems) or homogenized for immunoblot/immunoprecipitation analysis

Primary myoblast (satellite cell) isolation

Primary myoblasts were isolated from hindlimb muscles using the MACS satellite cell isolation kit (Miltenyi Biotec) according to the manufacturer's instructions. Briefly, dissected hindlimb muscles were rinsed in PBS, cleaned and then minced using razor blades in DMEM. Minced muscles were treated with 0.1% Pronase with slow stirring for 1 h at 37 °C followed by trituration in DMEM (+10% FBS, 100 units/ml penicillin G, 100 mg/ml streptomycin). Triturated muscle solution was passed through a Steriflip 100-μm vacuum filter and centrifuged at 900 × *g* for 5 min. The resulting pellet was washed in PBS and resuspended in ACK lysing buffer for 2 min at room temperature to lyse red blood cells. At the end of the incubation, samples were centrifuged at 900 × *g* for 5 min, and the pellet was resuspended with the addition of a satellite cell isolation kit followed by a 15-min incubation on ice. MACS buffer was added, and samples were applied to LS columns in a MACS magnetic field. Flowthrough containing satellite cells was collected, centrifuged at 900 × *g* for 5 min, and resuspended in growth medium (Ham's F10, 20% FBS, 5 ng/ml basic fibroblast growth factor, 100 units/ml penicillin G, 100 mg/ml streptomycin) on collagen-coated (bovine collagen I; Gibco) dishes.

Cell culture

All cultured cells were maintained in a humidified incubator with 5% CO_2 at 37 °C. Primary myoblasts were cultured in growth medium (Ham's F10, 20% FBS, 5 ng/ml basic fibroblast growth factor, 100 units/ml penicillin G, 100 mg/ml streptomycin) on collagen-coated (bovine collagen I; Gibco) dishes. Myoblasts were differentiated on dishes coated with entactin–collagen IV–laminin (Upstate Biotechnology) in growth medium, allowed to adhere, and then switched to differentiation medium (DMEM, 1% insulin–transferrin–selenium A (Invitrogen), 100 units/ml penicillin G, and 100 mg/ml streptomycin).

Immunoprecipitation

Primary myoblasts or electroporated muscles were homogenized in immunoprecipitation (IP) buffer (50 mM HEPES, 125 mM NaCl, 5 mM EDTA, 0.5% Nonidet P-40, 1 mM DTT, complete mini protease inhibitor mixture (Roche)). Homogenate was further lysed by sonication on ice five times at 0.5% output for 10 s and then passed through a 27-gauge syringe five times. Insoluble components were removed by centrifugation at 13,000 rpm for 15 min. The resulting supernatant was collected, and concentration of soluble proteins was determined using a bicinchoninic acid assay. 10% of lysate was removed to be used as the input sample, and M2 FLAG magnetic beads (Sigma) for IP from electroporated muscle or PABPN1 antibody (22) and control rabbit IgG for IP of endogenous PABPN1 were added to soluble cell lysates. The samples were incubated on an end-over-end rotator at 4 °C overnight. For endogenous PABPN1 immunoprecipitation, protein G magnetic beads (Dynabeads; Invitrogen) were added to the lysate for 1 h and incubated end-over-end at room temperature. The beads were then magnetized and washed three times with cold IP buffer. The washed beads were either submitted for mass spectrometric analysis or used for immunoblotting. To immunoblot IP samples, the proteins were eluted with reducing sample buffer (250 mM Tris-HCl, 500 mM DTT, 10% SDS, 0.5% bromphenol blue, 50% glycerol).

Immunoblotting

Cell lysates were prepared in radioimmunoprecipitation assay buffer with cOmplete protease inhibitor tablet (Roche Applied Science). Protein concentrations were measured using bicinchoninic acid assay, and equal total protein amounts were boiled in reducing sample buffer and resolved on 4–20% Criterion TGX polyacrylamide gels (Bio-Rad). Separated proteins were electrophoretically transferred to nitrocellulose membranes and incubated in blocking buffer (5% nonfat dry milk in TBS-Tween (0.1%)) for 1 h. Blocked blots were incubated overnight at 4 °C in primary antibody diluted in blocking buffer. Primary antibodies were detected using species-specific secondary antibodies conjugated to horseradish peroxidase plus incubation in enhanced chemiluminescence substrate (ECL, Sigma). Chemiluminescent signals were detected by exposing blots to autoradiography film (Daigger) or a Bio-Rad ChemiDoc imaging system. Primary antibodies used in this study: FLAG-M2 (1:1000, Sigma, F1804), HSP90 (1:4000, Santa Cruz, sc-13119), alanine (1:3000) (36), PABPN1 (1:3000) (22), hnRNPUL2 (1:1000, Bethyl, A304–619A), PABPC1 (1:2000, Abcam, ab21060), TDP-43 (1:2000, Proteintech, 10782-2-AP), and Progranulin (1:2000, Novus Biologicals, 26320002).

Liquid chromatography and tandem MS

We performed on-bead MS to identify PABPN1-interacting proteins. Lysate from muscles electroporated with each plasmid were pooled prior to immunoprecipitation to generate one

sample per plasmid. Following wash steps from the immunoprecipitation, Dynabeads from control and FLAG-PABPN1 immunoprecipitates were resuspended in 8 M urea, 100 mM $NaHPO_4$, pH 8.5 (50 μl final volume) and treated with 1 mM DTT at 25 °C for 30 min, followed by 5 mM iodoacetimide at 25 °C for 30 min in the dark. The samples were then diluted to 1 M urea with 50 mM ammonium bicarbonate (final volume, 400 μl) and digested with lysyl endopeptidase (Wako; final concentration, 1.25 ng/μl) at 25 °C for 4 h and further digested overnight with trypsin (Promega; final concentration, 1.25 ng/μl) at 25 °C. The resulting peptides were desalted with a Sep-Pak C18 column (Waters) and dried under vacuum. Each sample was resuspended in loading buffer (0.1% formic acid, 0.03% TFA, 1% acetonitrile) and analyzed independently by reverse-phase LC-MS/MS as essentially previously described with slight modification (88). Briefly, peptide mixtures were loaded onto a C18 nano-LC column (75-μm-inner diameter, 15-cm-long, 1.9-μm resin from Dr. Maisch GmbH) and eluted over a 5–30% gradient (buffer A: 0.1% formic acid; buffer B: 0.1% formic acid in 100% AcN). Eluates were monitored in a MS survey scan followed by 10 data-dependent MS/MS scans on a Q-Exactive plus Orbitrap mass spectrometer (Thermo Scientific, San Jose, CA). The acquired MS/MS spectra were searched against a concatenated target decoy mouse reference database (version 62) of the National Center for Biotechnology Information (downloaded November 14, 2013, with 30,267 target entries) using the SEQUEST Sorcerer algorithm (version 4.3.0, SAGE-N). Search parameters included: fully tryptic restriction, parent ion mass tolerance (± 50 ppm), up to two missed trypsin cleavages, and dynamic modifications for oxidized Met (+15.9949 Da). The peptides were classified by charge state and first filtered by mass accuracy (10 ppm for high-resolution MS) and then dynamically by increasing XCorr and Δ*Cn* values to reduce protein false discovery rate to less than 1%. If peptides were shared by multiple members of a protein family, the matched members were clustered into a single group in which each protein identified by a unique peptide represented a subgroup.

GO enrichment and network analysis

Functional enrichment of the proteins detected with Ala-10 PABPN1 or Ala-17 PABPN1 was determined using the GO-Elite (v1.2.5) package (89). The set of total proteins identified was used as the background. The *Z* score determines overrepresentation of ontologies in a module, and the permutation *p* value was used to assess the significance of the *Z* score cutoff of 1.96 and the *p* value cutoff 0.05, with a minimum of 5 proteins/category used as filters in pruning the ontologies. Horizontal bar graphs were plotted in *R*. The networks were constructed using the circlize package in *R*.

Immunohistochemistry

For detection of TDP-43, muscle sections of rectus femoris from 3-month-old mice were permeabilized in 0.3% Triton X-100 in PBS at room temperature (15 min), incubated in blocking buffer (0.3% BSA, 0.1% Triton X-100 in PBS) at room temperature (1–2 h), and incubated in primary α-TDP-43 (1:500, Proteintech, 10782-2-AP) and α-Dystrophin (1:100, Sigma, D8168) diluted in 0.5× blocking buffer in PBS at 4 °C (overnight). The slides were washed in 0.5× blocking buffer and incubated in FITC-conjugated donkey anti-rabbit IgG and Texas red-conjugated donkey anti-mouse IgG (Jackson ImmunoResearch Laboratories) diluted 1:500 in 0.5× blocking buffer at room temperature (1 h). The slides were washed in 0.5× blocking buffer, incubated in DAPI (1 μg/ml in PBS) to visualize nuclei, and mounted with Vectashield anti-fade mounting medium (Vector Laboratories). To remove soluble proteins, the slides were incubated at room temperature in 1 M KCl in HPEM buffer (30 mM HEPES, 65 mM PIPES, 10 mM EDTA, 2 mM $MgCl_2$, pH 6.9) for 1 h after permeabilization and before blocking.

Glycerol density gradients

Myotubes were lysed in native lysis buffer (10 mM HEPES, pH 7.5, 2 mM $MgCl_2$, 10 mM KCl, 0.5% Nonidet P-40, 0.5 mM EDTA, 150 mM NaCl, 1 mM DTT, and cOmplete Protease inhibitor mixture (Invitrogen)). Cell lysate (1.5 mg in 300 μl of volume) was layered onto 10–30% glycerol gradients (10 mM HEPES, pH 7.5, 2 mM $MgCl_2$, 10 mM KCl, 0.5 mM EDTA, and 150 mM NaCl) in 14 × 89-mm tubes (Beckman Coulter), and spun in a SW41Ti rotor (Beckman Coulter) at 30,000 × rpm for 16 h at 4 °C. Gradients were separated into 500-μl fractions top to bottom and used for immunoblotting.

Solubility assay

Myotubes were lysed in cold lysis buffer (50 mM Tris, pH 8, 150 mM NaCl, 1% Igepal CA-630) and incubated on ice with for 5 min. Lysates were sonicated with three 5-s pulses in a benchtop Branson sonicator (20% output) followed by centrifugation at 13,000 rpm at 4 °C for 20 min. The supernatant was collected as the soluble fraction, and the pellet was washed once with cold PBS and centrifuged for 10 min at 4 °C. The resulting pellet represented the insoluble fraction and was resuspended in 8 M urea, 2% SDS. Immunoblot analysis was performed on the soluble and insoluble fractions.

RNA isolation and reverse transcription

Total RNA was isolated using TRIzol reagent (Invitrogen) according to the manufacturer's protocol and treated with DNase I (Invitrogen). RNA was reverse-transcribed to cDNA using random hexamers and Moloney murine leukemia virus reverse transcriptase (Invitrogen). One microgram of RNA was used for each reverse transcription reaction and was then employed for quantitative real time PCR.

Quantitative real-time PCR

Relative mRNA levels were measured by quantitative PCR analysis of triplicate samples of 10 ng of cDNA with QuantiTect SYBR Green Master Mix on an Applied Biosystems StepOne Plus real time PCR machine (ABI). Fold change was calculated using the ΔΔ*Ct* method. The *Gapdh* transcript was used as the normalizer for the first Δ*Ct* and to primers sets for the coding sequence of the specific target for the second Δ*Ct*. Statistical significance was determined using Student's *t* test.

Glucose uptake assay

Glucose uptake was measured using a glucose uptake cell-based assay kit (catalog no. 600470) from Cayman Chemical as

per the manufacturer's instructions. Briefly, myoblasts and myotubes were grown in black, clear-bottomed 96-well plates and treated for 6 h with medium containing 200 μg/ml of the fluorescent deoxyglucose analog (2-NBDG) provided with the kit. Following this treatment, supernatant was aspirated, and cell-based assay buffer was added without disturbing the monolayer of cells. 2-NBDG taken up by the cells was detected using a Biotek microplate reader with filters designed to detect fluorescein (excitation/emission = 485/535 nm).

PGRN uptake assay

Myoblasts and myotubes were incubated for 16 h with recombinant N-TAP or C-TAP human Progranulin (a kind gift from the Kukar Lab, Emory University) (54). At the end of the incubation, the cells were washed three times with PBS and lysed in radioimmunoprecipitation assay buffer followed by immunoblotting to detect human PGRN.

Statistical analysis

All *error bars* represent standard error of the mean with statistical significance being determined with a Student's t test using GraphPad Prism7. In all cases samples with $p < 0.05$ were considered to be statistically significant.

Author contributions—A. B., G. K. P., K. E. V., and A. H. C. conceptualization; A. B. and Q. D. data curation; A. B., B.L.P., Q. D., and A. H. C. formal analysis; A. B., B.L.P., K. E. V., and A. H. C. investigation; A. B. and K. E. V. methodology; A. B., K. E. V., and A. H. C. writing-original draft; A. B. and A. H. C. project administration; A. B., G. K. P., K. E. V., and A. H. C. writing-review and editing; Q. D. software; N.T.S., G. K. P., K. E. V., and A. H. C. supervision; A. H. C. funding acquisition.

Acknowledgments—We acknowledge the Kukar lab at Emory University for providing recombinant N-TAP and C-TAP human progranulin and anti-human progranulin antibody. Proteomic analysis was performed by the Emory University School of Medicine Integrated Proteomics Core.

References

1. Amiel, J., Trochet, D., Clément-Ziza, M., Munnich, A., and Lyonnet, S. (2004) Polyalanine expansions in human. *Hum. Mol. Genet.* **13,** R235–R243 CrossRef Medline
2. Messaed, C., and Rouleau, G. A. (2009) Molecular mechanisms underlying polyalanine diseases. *Neurobiol. Dis.* **34,** 397–405 CrossRef Medline
3. Brais, B., Bouchard, J. P., Xie, Y. G., Rochefort, D. L., Chrétien, N., Tomé, F. M., Lafrenière, R. G., Rommens, J. M., Uyama, E., Nohira, O., Blumen, S., Korczyn, A. D., Heutink, P., Mathieu, J., Duranceau, A., *et al.* (1998) Short GCG expansions in the PABP2 gene cause oculopharyngeal muscular dystrophy. *Nat. Genet.* **18,** 164–167 CrossRef Medline
4. Jouan, L., Rocheford, D., Szuto, A., Carney, E., David, K., Dion, P. A., and Rouleau, G. A. (2014) An 18 alanine repeat in a severe form of oculopharyngeal muscular dystrophy. *Can. J. Neurol. Sci.* **41,** 508–511 CrossRef Medline
5. Albrecht, A., and Mundlos, S. (2005) The other trinucleotide repeat: polyalanine expansion disorders. *Curr. Opin. Genet. Dev.* **15,** 285–293 CrossRef Medline
6. Uyama, E., Tsukahara, T., Goto, K., Kurano, Y., Ogawa, M., Kim, Y. J., Uchino, M., and Arahata, K. (2000) Nuclear accumulation of expanded PABP2 gene product in oculopharyngeal muscular dystrophy. *Muscle Nerve* **23,** 1549–1554 CrossRef Medline
7. Calado, A., Tomé, F. M., Brais, B., Rouleau, G. A., Kühn, U., Wahle, E., and Carmo-Fonseca, M. (2000) Nuclear inclusions in oculopharyngeal muscular dystrophy consist of poly(A) binding protein 2 aggregates which sequester poly(A) RNA. *Hum. Mol. Genet.* **9,** 2321–2328 CrossRef Medline
8. Messaed, C., Dion, P. A., Abu-Baker, A., Rochefort, D., Laganiere, J., Brais, B., and Rouleau, G. A. (2007) Soluble expanded PABPN1 promotes cell death in oculopharyngeal muscular dystrophy. *Neurobiol. Dis.* **26,** 546–557 CrossRef Medline
9. Mankodi, A., Wheeler, T. M., Shetty, R., Salceies, K. M., Becher, M. W., and Thornton, C. A. (2012) Progressive myopathy in an inducible mouse model of oculopharyngeal muscular dystrophy. *Neurobiol. Dis.* **45,** 539–546 CrossRef Medline
10. Dion, P., Shanmugam, V., Gaspar, C., Messaed, C., Meijer, I., Toulouse, A., Laganiere, J., Roussel, J., Rochefort, D., Laganiere, S., Allen, C., Karpati, G., Bouchard, J. P., Brais, B., and Rouleau, G. A. (2005) Transgenic expression of an expanded (GCG)13 repeat PABPN1 leads to weakness and coordination defects in mice. *Neurobiol. Dis.* **18,** 528–536 CrossRef Medline
11. Berciano, M. T., Villagra, N. T., Ojeda, J. L., Navascues, J., Gomes, A., Lafarga, M., and Carmo-Fonseca, M. (2004) Oculopharyngeal muscular dystrophy-like nuclear inclusions are present in normal magnocellular neurosecretory neurons of the hypothalamus. *Hum. Mol. Genet.* **13,** 829–838 CrossRef Medline
12. Villagra, N. T., Bengoechea, R., Vaqué, J. P., Llorca, J., Berciano, M. T., and Lafarga, M. (2008) Nuclear compartmentalization and dynamics of the poly(A)-binding protein nuclear 1 (PABPN1) inclusions in supraoptic neurons under physiological and osmotic stress conditions. *Mol. Cell. Neurosci.* **37,** 622–633 CrossRef Medline
13. Corbeil-Girard, L. P., Klein, A. F., Sasseville, A. M., Lavoie, H., Dicaire, M. J., Saint-Denis, A., Pagé, M., Duranceau, A., Codère, F., Bouchard, J. P., Karpati, G., Rouleau, G. A., Massie, B., Langelier, Y., and Brais, B. (2005) PABPN1 overexpression leads to upregulation of genes encoding nuclear proteins that are sequestered in oculopharyngeal muscular dystrophy nuclear inclusions. *Neurobiol. Dis.* **18,** 551–567 CrossRef Medline
14. Fan, X., Messaed, C., Dion, P., Laganiere, J., Brais, B., Karpati, G., and Rouleau, G. A. (2003) HnRNP A1 and A/B interaction with PABPN1 in oculopharyngeal muscular dystrophy. *Can. J. Neurol. Sci.* **30,** 244–251 CrossRef Medline
15. Apponi, L. H., Corbett, A. H., and Pavlath, G. K. (2013) Control of mRNA stability contributes to low levels of nuclear poly(A) binding protein 1 (PABPN1) in skeletal muscle. *Skeletal Muscle* **3,** 23 CrossRef Medline
16. Phillips, B. L., Banerjee, A., Sanchez, B. J., Di Marco, S., Gallouzi, I. E., Pavlath, G. K., and Corbett, A. H. (2018) Post-transcriptional regulation of Pabpn1 by the RNA binding protein HuR. *Nucleic Acids Res.* **46,** 7643–7661 CrossRef Medline
17. Gerstberger, S., Hafner, M., Ascano, M., and Tuschl, T. (2014) Evolutionary conservation and expression of human RNA-binding proteins and their role in human genetic disease. *Adv. Exp. Med. Biol.* **825,** 1–55 CrossRef Medline
18. Banerjee, A., Apponi, L. H., Pavlath, G. K., and Corbett, A. H. (2013) PABPN1: molecular function and muscle disease. *FEBS J.* **280,** 4230–4250 CrossRef Medline
19. Kühn, U., Gündel, M., Knoth, A., Kerwitz, Y., Rüdel, S., and Wahle, E. (2009) Poly(A) tail length is controlled by the nuclear poly(A)-binding protein regulating the interaction between poly(A) polymerase and the cleavage and polyadenylation specificity factor. *J. Biol. Chem.* **284,** 22803–22814 CrossRef Medline
20. Jenal, M., Elkon, R., Loayza-Puch, F., van Haaften, G., Kühn, U., Menzies, F. M., Oude Vrielink, J. A., Bos, A. J., Drost, J., Rooijers, K., Rubinsztein, D. C., and Agami, R. (2012) The poly(A)-binding protein nuclear 1 suppresses alternative cleavage and polyadenylation sites. *Cell* **149,** 538–553 CrossRef Medline
21. de Klerk, E., Venema, A., Anvar, S. Y., Goeman, J. J., Hu, O., Trollet, C., Dickson, G., den Dunnen, J. T., van der Maarel, S. M., Raz, V., and 't Hoen, P. A. (2012) Poly(A) binding protein nuclear 1 levels affect alternative polyadenylation. *Nucleic Acids Res.* **40,** 9089–9101 CrossRef Medline
22. Apponi, L. H., Leung, S. W., Williams, K. R., Valentini, S. R., Corbett, A. H., and Pavlath, G. K. (2010) Loss of nuclear poly(A)-binding protein 1 causes

defects in myogenesis and mRNA biogenesis. *Hum. Mol. Genet.* **19,** 1058–1065 CrossRef Medline
23. Calado, A., Kutay, U., Kühn, U., Wahle, E., and Carmo-Fonseca, M. (2000) Deciphering the cellular pathway for transport of poly(A)-binding protein II. *RNA* **6,** 245–256 CrossRef Medline
24. Ishigaki, Y., Li, X., Serin, G., and Maquat, L. E. (2001) Evidence for a pioneer round of mRNA translation: mRNAs subject to nonsense-mediated decay in mammalian cells are bound by CBP80 and CBP20. *Cell* **106,** 607–617 CrossRef Medline
25. Abu-Baker, A., and Rouleau, G. A. (2007) Oculopharyngeal muscular dystrophy: recent advances in the understanding of the molecular pathogenic mechanisms and treatment strategies. *Biochim. Biophys. Acta* **1772,** 173–185 CrossRef Medline
26. Goodman, F. R., Mundlos, S., Muragaki, Y., Donnai, D., Giovannucci-Uzielli, M. L., Lapi, E., Majewski, F., McGaughran, J., McKeown, C., Reardon, W., Upton, J., Winter, R. M., Olsen, B. R., and Scambler, P. J. (1997) Synpolydactyly phenotypes correlate with size of expansions in HOXD13 polyalanine tract. *Proc. Natl. Acad. Sci. U.S.A.* **94,** 7458–7463 CrossRef Medline
27. Tavanez, J. P., Bengoechea, R., Berciano, M. T., Lafarga, M., Carmo-Fonseca, M., and Enguita, F. J. (2009) Hsp70 chaperones and type I PRMTs are sequestered at intranuclear inclusions caused by polyalanine expansions in PABPN1. *PLoS One* **4,** e6418 CrossRef Medline
28. Kim, Y. J., Noguchi, S., Hayashi, Y. K., Tsukahara, T., Shimizu, T., and Arahata, K. (2001) The product of an oculopharyngeal muscular dystrophy gene, poly(A)-binding protein 2, interacts with SKIP and stimulates muscle-specific gene expression. *Hum. Mol. Genet.* **10,** 1129–1139 CrossRef Medline
29. Banerjee, A., Vest, K. E., Pavlath, G. K., and Corbett, A. H. (2017) Nuclear poly(A) binding protein 1 (PABPN1) and Matrin3 interact in muscle cells and regulate RNA processing. *Nucleic Acids Res.* **45,** 10706–10725 CrossRef Medline
30. Küsters, B., van Hoeve, B. J., Schelhaas, H. J., Ter Laak, H., van Engelen, B. G., and Lammens, M. (2009) TDP-43 accumulation is common in myopathies with rimmed vacuoles. *Acta Neuropathol.* **117,** 209–211 CrossRef Medline
31. Chou, C. C., Alexeeva, O. M., Yamada, S., Pribadi, A., Zhang, Y., Mo, B., Williams, K. R., Zarnescu, D. C., and Rossoll, W. (2015) PABPN1 suppresses TDP-43 toxicity in ALS disease models. *Hum. Mol. Genet.* **24,** 5154–5173 CrossRef Medline
32. Vogler, T. O., Wheeler, J. R., Nguyen, E. D., Hughes, M. P., Britson, K. A., Lester, E., Rao, B., Betta, N. D., Whitney, O. N., Ewachiw, T. E., Gomes, E., Shorter, J., Lloyd, T. E., Eisenberg, D. S., Taylor, J. P., *et al.* (2018) TDP-43 and RNA form amyloid-like myo-granules in regenerating muscle. *Nature* **563,** 508–513 CrossRef Medline
33. Vest, K. E., Phillips, B. L., Banerjee, A., Apponi, L. H., Dammer, E. B., Xu, W., Zheng, D., Yu, J., Tian, B., Pavlath, G. K., and Corbett, A. H. (2017) Novel mouse models of oculopharyngeal muscular dystrophy (OPMD) reveal early onset mitochondrial defects and suggest loss of PABPN1 may contribute to pathology. *Hum. Mol. Genet.* **26,** 3235–3252 CrossRef Medline
34. Davies, J. E., Wang, L., Garcia-Oroz, L., Cook, L. J., Vacher, C., O'Donovan, D. G., and Rubinsztein, D. C. (2005) Doxycycline attenuates and delays toxicity of the oculopharyngeal muscular dystrophy mutation in transgenic mice. *Nat. Med.* **11,** 672–677 CrossRef Medline
35. Randolph, M. E., Luo, Q., Ho, J., Vest, K. E., Sokoloff, A. J., and Pavlath, G. K. (2014) Ageing and muscular dystrophy differentially affect murine pharyngeal muscles in a region-dependent manner. *J. Physiol.* **592,** 5301–5315 CrossRef Medline
36. Vest, K. E., Apponi, L. H., Banerjee, A., Pavlath, G. K., and Corbett, A. H. (2015) An antibody to detect alanine-expanded PABPN1: a new tool to study oculopharyngeal muscular dystrophy. *J. Neuromuscul. Dis.* **2,** 439–446 CrossRef Medline
37. Kühn, U., Nemeth, A., Meyer, S., and Wahle, E. (2003) The RNA binding domains of the nuclear poly(A)-binding protein. *J. Biol. Chem.* **278,** 16916–16925 CrossRef Medline
38. Kühn, U., and Wahle, E. (2004) Structure and function of poly(A) binding proteins. *Biochim. Biophys. Acta* **1678,** 67–84 CrossRef Medline
39. Neumann, M., Sampathu, D. M., Kwong, L. K., Truax, A. C., Micsenyi, M. C., Chou, T. T., Bruce, J., Schuck, T., Grossman, M., Clark, C. M., McCluskey, L. F., Miller, B. L., Masliah, E., Mackenzie, I. R., Feldman, H., *et al.* (2006) Ubiquitinated TDP-43 in frontotemporal lobar degeneration and amyotrophic lateral sclerosis. *Science* **314,** 130–133 CrossRef Medline
40. Cykowski, M. D., Powell, S. Z., Appel, J. W., Arumanayagam, A. S., Rivera, A. L., and Appel, S. H. (2018) Phosphorylated TDP-43 (pTDP-43) aggregates in the axial skeletal muscle of patients with sporadic and familial amyotrophic lateral sclerosis. *Acta Neuropathol. Commun.* **6,** 28 CrossRef Medline
41. Cortese, A., Plagnol, V., Brady, S., Simone, R., Lashley, T., Acevedo-Arozena, A., de Silva, R., Greensmith, L., Holton, J., Hanna, M. G., Fisher, E. M., and Fratta, P. (2014) Widespread RNA metabolism impairment in sporadic inclusion body myositis TDP43-proteinopathy. *Neurobiol. Aging* **35,** 1491–1498 CrossRef Medline
42. Cutler, A. A., Corbett, A. H., and Pavlath, G. K. (2017) Biochemical isolation of myonuclei from mouse skeletal muscle tissue. *Bio Protocol* **7,** e2654 Medline
43. Chal, J., and Pourquié, O. (2017) Making muscle: skeletal myogenesis *in vivo* and *in vitro*. *Development* **144,** 2104–2122 CrossRef Medline
44. Cohen, T. J., Hwang, A. W., Unger, T., Trojanowski, J. Q., and Lee, V. M. (2012) Redox signalling directly regulates TDP-43 via cysteine oxidation and disulphide cross-linking. *EMBO J.* **31,** 1241–1252 CrossRef Medline
45. Tollervey, J. R., Curk, T., Rogelj, B., Briese, M., Cereda, M., Kayikci, M., König, J., Hortobágyi, T., Nishimura, A. L., Zupunski, V., Patani, R., Chandran, S., Rot, G., Zupan, B., Shaw, C. E., *et al.* (2011) Characterizing the RNA targets and position-dependent splicing regulation by TDP-43. *Nat. Neurosci.* **14,** 452–458 CrossRef Medline
46. Ricketts, T., McGoldrick, P., Fratta, P., de Oliveira, H. M., Kent, R., Phatak, V., Brandner, S., Blanco, G., Greensmith, L., Acevedo-Arozena, A., and Fisher, E. M. (2014) A nonsense mutation in mouse Tardbp affects TDP43 alternative splicing activity and causes limb-clasping and body tone defects. *PLoS One* **9,** e85962 CrossRef Medline
47. Afroz, T., Hock, E. M., Ernst, P., Foglieni, C., Jambeau, M., Gilhespy, L. A. B., Laferriere, F., Maniecka, Z., Plückthun, A., Mittl, P., Paganetti, P., Allain, F. H. T., and Polymenidou, M. (2017) Functional and dynamic polymerization of the ALS-linked protein TDP-43 antagonizes its pathologic aggregation. *Nat. Commun.* **8,** 45 CrossRef Medline
48. Mohagheghi, F., Prudencio, M., Stuani, C., Cook, C., Jansen-West, K., Dickson, D. W., Petrucelli, L., and Buratti, E. (2016) TDP-43 functions within a network of hnRNP proteins to inhibit the production of a truncated human SORT1 receptor. *Hum. Mol. Genet.* **25,** 534–545 CrossRef Medline
49. Ariga, M., Nedachi, T., Katagiri, H., and Kanzaki, M. (2008) Functional role of sortilin in myogenesis and development of insulin-responsive glucose transport system in C2C12 myocytes. *J. Biol. Chem.* **283,** 10208–10220 CrossRef Medline
50. Shi, J., and Kandror, K. V. (2005) Sortilin is essential and sufficient for the formation of Glut4 storage vesicles in 3T3-L1 adipocytes. *Dev. Cell* **9,** 99–108 CrossRef Medline
51. Carrasquillo, M. M., Nicholson, A. M., Finch, N., Gibbs, J. R., Baker, M., Rutherford, N. J., Hunter, T. A., DeJesus-Hernandez, M., Bisceglio, G. D., Mackenzie, I. R., Singleton, A., Cookson, M. R., Crook, J. E., Dillman, A., Hernandez, D., *et al.* (2010) Genome-wide screen identifies rs646776 near sortilin as a regulator of progranulin levels in human plasma. *Am. J. Hum. Genet.* **87,** 890–897 CrossRef Medline
52. Hu, F., Padukkavidana, T., Vægter, C. B., Brady, O. A., Zheng, Y., Mackenzie, I. R., Feldman, H. H., Nykjaer, A., and Strittmatter, S. M. (2010) Sortilin-mediated endocytosis determines levels of the frontotemporal dementia protein, progranulin. *Neuron* **68,** 654–667 CrossRef Medline
53. Richter, E. A., and Hargreaves, M. (2013) Exercise, GLUT4, and skeletal muscle glucose uptake. *Physiol. Rev.* **93,** 993–1017 CrossRef Medline
54. Holler, C. J., Taylor, G., Deng, Q., and Kukar, T. (2017) Intracellular proteolysis of progranulin generates stable, lysosomal granulins that are hap-

loinsufficient in patients with frontotemporal dementia caused by *GRN* mutations. *eNeuro* **4,** ENEURO.0100-17.2017 Medline
55. Zheng, Y., Brady, O. A., Meng, P. S., Mao, Y., and Hu, F. (2011) C-terminus of progranulin interacts with the beta-propeller region of sortilin to regulate progranulin trafficking. *PLoS One* **6,** e21023 CrossRef Medline
56. Tavanez, J. P., Calado, P., Braga, J., Lafarga, M., and Carmo-Fonseca, M. (2005) In vivo aggregation properties of the nuclear poly(A)-binding protein PABPN1. *RNA* **11,** 752–762 CrossRef Medline
57. Raz, V., Abraham, T., van Zwet, E. W., Dirks, R. W., Tanke, H. J., and van der Maarel, S. M. (2011) Reversible aggregation of PABPN1 pre-inclusion structures. *Nucleus* **2,** 208–218 CrossRef Medline
58. Fronz, K., Güttinger, S., Burkert, K., Kühn, U., Stöhr, N., Schierhorn, A., and Wahle, E. (2011) Arginine methylation of the nuclear poly(a) binding protein weakens the interaction with its nuclear import receptor, transportin. *J. Biol. Chem.* **286,** 32986–32994 CrossRef Medline
59. Aktas, T., Avsar Ilik, I., Maticzka, D., Bhardwaj, V., Pessoa Rodrigues, C., Mittler, G., Manke, T., Backofen, R., and Akhtar, A. (2017) DHX9 suppresses RNA processing defects originating from the Alu invasion of the human genome. *Nature* **544,** 115–119 CrossRef Medline
60. Moore, K. S., Yagci, N., van Alphen, F., Paolini, N. A., Horos, R., Held, N. M., Houtkooper, R. H., van den Akker, E., Meijer, A. B., 't Hoen, P. A. C., and von Lindern, M. (2018) Csde1 binds transcripts involved in protein homeostasis and controls their expression in an erythroid cell line. *Sci. Rep.* **8,** 2628 CrossRef Medline
61. Ma, W. J., Chung, S., and Furneaux, H. (1997) The Elav-like proteins bind to AU-rich elements and to the poly(A) tail of mRNA. *Nucleic Acids Res.* **25,** 3564–3569 CrossRef Medline
62. Fan, X. C., and Steitz, J. A. (1998) Overexpression of HuR, a nuclear-cytoplasmic shuttling protein, increases the *in vivo* stability of ARE-containing mRNAs. *EMBO J.* **17,** 3448–3460 CrossRef Medline
63. Medghalchi, S. M., Frischmeyer, P. A., Mendell, J. T., Kelly, A. G., Lawler, A. M., and Dietz, H. C. (2001) Rent1, a trans-effector of nonsense-mediated mRNA decay, is essential for mammalian embryonic viability. *Hum. Mol. Genet.* **10,** 99–105 CrossRef Medline
64. Kim, Y. K., Furic, L., Desgroseillers, L., and Maquat, L. E. (2005) Mammalian Staufen1 recruits Upf1 to specific mRNA 3′UTRs so as to elicit mRNA decay. *Cell* **120,** 195–208 CrossRef Medline
65. Koh, H. R., Xing, L., Kleiman, L., and Myong, S. (2014) Repetitive RNA unwinding by RNA helicase A facilitates RNA annealing. *Nucleic Acids Res.* **42,** 8556–8564 CrossRef Medline
66. Kamelgarn, M., Chen, J., Kuang, L., Arenas, A., Zhai, J., Zhu, H., and Gal, J. (2016) Proteomic analysis of FUS interacting proteins provides insights into FUS function and its role in ALS. *Biochim. Biophys. Acta* **1862,** 2004–2014 CrossRef Medline
67. Chi, B., O'Connell, J. D., Yamazaki, T., Gangopadhyay, J., Gygi, S. P., and Reed, R. (2018) Interactome analyses revealed that the U1 snRNP machinery overlaps extensively with the RNAP II machinery and contains multiple ALS/SMA-causative proteins. *Sci. Rep.* **8,** 8755 CrossRef Medline
68. Pauzner, R., Blatt, I., Mouallem, M., Ben-David, E., Farfel, Z., and Sadeh, M. (1991) Mitochondrial abnormalities in oculopharyngeal muscular dystrophy. *Muscle Nerve* **14,** 947–952 CrossRef Medline
69. Chartier, A., Klein, P., Pierson, S., Barbezier, N., Gidaro, T., Casas, F., Carberry, S., Dowling, P., Maynadier, L., Bellec, M., Oloko, M., Jardel, C., Moritz, B., Dickson, G., Mouly, V., *et al.* (2015) Mitochondrial dysfunction reveals the role of mRNA poly(A) tail regulation in oculopharyngeal muscular dystrophy pathogenesis. *PLoS Genet.* **11,** e1005092 CrossRef Medline
70. Franco-Iborra, S., Vila, M., and Perier, C. (2018) Mitochondrial quality control in neurodegenerative diseases: focus on Parkinson's disease and Huntington's disease. *Front. Neurosci.* **12,** 342 CrossRef Medline
71. Toriumi, K., Oma, Y., Kino, Y., Futai, E., Sasagawa, N., and Ishiura, S. (2008) Expression of polyalanine stretches induces mitochondrial dysfunction. *J. Neurosci. Res.* **86,** 1529–1537 CrossRef Medline
72. Toriumi, K., Oma, Y., Mimoto, A., Futai, E., Sasagawa, N., Turk, B., and Ishiura, S. (2009) Polyalanine tracts directly induce the release of cytochrome *c*, independently of the mitochondrial permeability transition pore, leading to apoptosis. *Genes Cells* **14,** 751–757 CrossRef Medline
73. Lopez-Gonzalez, R., Lu, Y., Gendron, T. F., Karydas, A., Tran, H., Yang, D., Petrucelli, L., Miller, B. L., Almeida, S., and Gao, F. B. (2016) Poly(GR) in C9ORF72-related ALS/FTD compromises mitochondrial function and increases oxidative stress and DNA damage in iPSC-derived motor neurons. *Neuron* **92,** 383–391 CrossRef Medline
74. Wang, W., Wang, L., Lu, J., Siedlak, S. L., Fujioka, H., Liang, J., Jiang, S., Ma, X., Jiang, Z., da Rocha, E. L., Sheng, M., Choi, H., Lerou, P. H., Li, H., and Wang, X. (2016) The inhibition of TDP-43 mitochondrial localization blocks its neuronal toxicity. *Nat. Med.* **22,** 869–878 CrossRef Medline
75. Davis, S. A., Itaman, S., Khalid-Janney, C. M., Sherard, J. A., Dowell, J. A., Cairns, N. J., and Gitcho, M. A. (2018) TDP-43 interacts with mitochondrial proteins critical for mitophagy and mitochondrial dynamics. *Neurosci. Lett.* **678,** 8–15 CrossRef Medline
76. Ling, S. C., Albuquerque, C. P., Han, J. S., Lagier-Tourenne, C., Tokunaga, S., Zhou, H., and Cleveland, D. W. (2010) ALS-associated mutations in TDP-43 increase its stability and promote TDP-43 complexes with FUS/TLS. *Proc. Natl. Acad. Sci. U.S.A.* **107,** 13318–13323 CrossRef Medline
77. Cohen, T. J., Lee, V. M., and Trojanowski, J. Q. (2011) TDP-43 functions and pathogenic mechanisms implicated in TDP-43 proteinopathies. *Trends Mol. Med.* **17,** 659–667 CrossRef Medline
78. Kim, S. H., Shanware, N. P., Bowler, M. J., and Tibbetts, R. S. (2010) Amyotrophic lateral sclerosis-associated proteins TDP-43 and FUS/TLS function in a common biochemical complex to co-regulate HDAC6 mRNA. *J. Biol. Chem.* **285,** 34097–34105 CrossRef Medline
79. Polymenidou, M., Lagier-Tourenne, C., Hutt, K. R., Huelga, S. C., Moran, J., Liang, T. Y., Ling, S. C., Sun, E., Wancewicz, E., Mazur, C., Kordasiewicz, H., Sedaghat, Y., Donohue, J. P., Shiue, L., Bennett, C. F., *et al.* (2011) Long pre-mRNA depletion and RNA missplicing contribute to neuronal vulnerability from loss of TDP-43. *Nat. Neurosci.* **14,** 459–468 CrossRef Medline
80. Johnson, J. O., Pioro, E. P., Boehringer, A., Chia, R., Feit, H., Renton, A. E., Pliner, H. A., Abramzon, Y., Marangi, G., Winborn, B. J., Gibbs, J. R., Nalls, M. A., Morgan, S., Shoai, M., Hardy, J., *et al.* (2014) Mutations in the Matrin 3 gene cause familial amyotrophic lateral sclerosis. *Nat. Neurosci.* **17,** 664–666 CrossRef Medline
81. Tada, M., Doi, H., Koyano, S., Kubota, S., Fukai, R., Hashiguchi, S., Hayashi, N., Kawamoto, Y., Kunii, M., Tanaka, K., Takahashi, K., Ogawa, Y., Iwata, R., Yamanaka, S., Takeuchi, H., *et al.* (2018) Matrin 3 is a component of neuronal cytoplasmic inclusions of motor neurons in sporadic amyotrophic lateral sclerosis. *Am. J. Pathol.* **188,** 507–514 CrossRef Medline
82. Weihl, C. C., Temiz, P., Miller, S. E., Watts, G., Smith, C., Forman, M., Hanson, P. I., Kimonis, V., and Pestronk, A. (2008) TDP-43 accumulation in inclusion body myopathy muscle suggests a common pathogenic mechanism with frontotemporal dementia. *J. Neurol. Neurosurg. Psychiatry* **79,** 1186–1189 CrossRef Medline
83. Lei, L., Ren, D., and Burton, Z. F. (1999) The RAP74 subunit of human transcription factor IIF has similar roles in initiation and elongation. *Mol. Cell. Biol.* **19,** 8372–8382 CrossRef Medline
84. Renz, A., and Fackelmayer, F. O. (1996) Purification and molecular cloning of the scaffold attachment factor B (SAF-B), a novel human nuclear protein that specifically binds to S/MAR-DNA. *Nucleic Acids Res.* **24,** 843–849 CrossRef Medline
85. Dahl, R., Wani, B., and Hayman, M. J. (1998) The Ski oncoprotein interacts with Skip, the human homolog of *Drosophila* Bx42. *Oncogene* **16,** 1579–1586 CrossRef Medline
86. Figueroa, J. D., and Hayman, M. J. (2004) Differential effects of the Ski-interacting protein (SKIP) on differentiation induced by transforming growth factor-β1 and bone morphogenetic protein-2 in C2C12 cells. *Exp. Cell Res.* **296,** 163–172 CrossRef Medline
87. Yamaguchi, A., and Takanashi, K. (2016) FUS interacts with nuclear matrix-associated protein SAFB1 as well as Matrin3 to regulate splicing and ligand-mediated transcription. *Sci. Rep.* **6,** 35195 CrossRef Medline

88. Donovan, L. E., Dammer, E. B., Duong, D. M., Hanfelt, J. J., Levey, A. I., Seyfried, N. T., and Lah, J. J. (2013) Exploring the potential of the platelet membrane proteome as a source of peripheral biomarkers for Alzheimer's disease. *Alzheimers Res. Ther.* **5,** 32 CrossRef Medline
89. Zambon, A. C., Gaj, S., Ho, I., Hanspers, K., Vranizan, K., Evelo, C. T., Conklin, B. R., Pico, A. R., and Salomonis, N. (2012) GO-Elite: a flexible solution for pathway and ontology over-representation. *Bioinformatics* **28,** 2209–2210 CrossRef Medline
90. Wobst, H. J., Delsing, L., Brandon, N. J., and Moss, S. J. (2017) Truncation of the TAR DNA-binding protein 43 is not a prerequisite for cytoplasmic relocalization, and is suppressed by caspase inhibition and by introduction of the A90V sequence variant. *PLoS One* **12,** e0177181 CrossRef Medline